Charles University
Faculty of Science
Department of Physical and Macromolecular Chemistry

Doctoral thesis

Microwave-assisted preparation of polymer materials

M.Sc. Sonia Bujok
Study programme: Macromolecular chemistry

Supervisor: Ing. Hynek Beneš, Ph.D.

Institute of Macromolecular Chemistry of the Czech Academy of Sciences
Department of Polymer Processing

Prague 2021

Univerzita Karlova
Přírodovědecká fakulta
Katedra fyzikální a makromolekulární chemie

Disertační práce

Příprava polymerních materiálů v mikrovlnném poli

M.Sc. Sonia Bujok

Studijní program: Makromolekulární chemie

Školitel: Ing. Hynek Beneš, Ph.D.

Ústav makromolekulární chemie AV ČR, v. v. i.
Oddělení: Zpracování polymerních materiálů

Praha 2021

Prohlášení:

Prohlašuji, že jsem předkládanou disertační práci vypracovala samostatně pod vedením školitele Ing. Hynka Beneše, Ph.D. a že jsem uvedla všechny použité informační zdroje a literaturu. Dále prohlašuji, že tato disertační práce ani její část nebyla předložena k získání jiného nebo stejného akademického titulu.

Declaration:

I hereby declare that I have written this doctoral thesis independently under the supervision of Ing. Hynek Beneš, Ph.D. and all the resources which were used have been cited. Results published in this thesis have not been used for gaining any other or equivalent academic degree.

Prague, 30.06.2021 Sonia Bujok

I would like to thank my supervisor Ing. Hynek Beneš, Ph.D. and all of my colleagues from Institute of Macromolecular Chemistry CAS, Institute of Inorganic Chemistry CAS and University of Chemistry and Technology in Prague for cooperation, help and their valuable contribution to this doctoral thesis.

Table of contents

Abstract

Bearing in mind environmental concerns and global trends in ecology, biodegradable polyesters have gained enormous attention as alternative to non-biodegradable, commercial polymers used mainly in packaging industry contributing to the worldwide environment pollution. However, substitution of conventional polymers with biodegradable polyesters is limited due to their inferior mechanical and barrier properties, which can be improved by the introduction of relatively small content of non-toxic nanofillers. Nevertheless, environmental pollution is not only affected by material itself, but also manufacturing and processing sector in terms of energy sustainability. In case of the latter, low energetic processes are nowadays preferential. Thus, using microwave irradiation as the more efficient energy source, which can lead to shortening of process time, has become currently investigated subject.

In this thesis, microwave-assisted *in-situ* synthesis of biodegradable nanocomposites based on polycaprolactone and non-toxic clay nanoparticles (layered double hydroxides) was studied and described in detail in four subsections (4.1-4.4).

The first subsection (4.1) describes one-pot synthesis of Mg^{2+}/Al^{3+} layered double hydroxides functionalized with highly microwave-absorbing ionic liquids. In order to improve homogeneity of the nanoparticles synthesized in the subsection 4.1, Ca^{2+}/Al^{3+} layered double hydroxides were prepared and further functionalized with one ionic liquid. These nanoparticles were subsequently used for the *in-situ* microwave-assisted ring opening polymerization of ε-caprolactone (subsection 4.2). This section describes also mechanism, kinetics and thermodynamics of the studied polymerization. Subsection 4.3 compares *in-situ* polymerization and melt-blending as two preparation methods of polycaprolactone nanocomposites and describes the effect of the ionic liquid-layered double hydroxides on their mechanical, thermal, and barrier properties. The influence of the alternative (antibacterial) ionic liquid-functionalized Zn^{2+}/Al^{3+} layered double hydroxides on the application-related properties of nanocomposites (barrier, bactericidal) was further described in the subsection 4.4, where the biodegradability of such prepared nanocomposites was also evaluated.

It has been demonstrated that microwave-assisted *in-situ* ring opening polymerization of ε-caprolactone in the presence of ionic liquid-layered double hydroxides is a sustainable route for biodegradable polycaprolactone nanocomposites, which have a high application potential for e.g. active bio-packaging.

Abstrakt

Vzhledem k současným celosvětovým snahám o snížení plastového znečištění životního prostředí, se biologicky odbouratelné polyestery dostávají do popředí zájmu jako alternativní materiály ke konvenčním (komerčním) polymerům, které mohou nacházet uplatnění např. v obalovém průmyslu. Značným omezením biologicky rozložitelných (především alifatických) polyesterů jsou jejich horší mechanické a bariérové vlastnosti, které lze však do určité míry vylepšit přídavkem relativně malého množství netoxických nanoplniv. Životní prostředí však není zatíženo pouze materiálem samotným, svou roli sehrává i energetická náročnost vlastního výrobního procesu a zpracovatelských postupů. V poslední době proto dochází k výraznému příklonu k nízkoenergetickým procesům. Využití mikrovlnného záření jako účinného zdroje energie, který může vést k výraznému zkrácení procesních časů, je tak v současné době předmětem intenzivního výzkumu.

V této disertační práci je ve čtyřech kapitolách (4.1-4.4) podrobně studována a popsána *in-situ* mikrovlnná syntéza biologicky odbouratelných nanokompozitů na bázi polykaprolaktonu a netoxických jílových nanočástic (vrstevnatých podvojných hydroxidů).

První kapitola (4.1) popisuje jednokrokovou syntézu vrstevnatých podvojných hydroxidů na bázi Mg^{2+}/Al^{3+} funkcionalizovaných iontovými kapalinami, které jsou schopny silně absorbovat mikrovlnné záření. Za účelem zlepšení homogenity nanočástic syntetizovaných v kapitole 4.1, byly dále připraveny vrstevnaté podvojné hydroxidy na bázi Ca^{2+}/Al^{3+}, které byly dále funkcionalizovány iontovou kapalinou. Tyto nanočástice byly následně použity pro *in-situ* mikrovlnnou polymeraci za otevření kruhu ε-kaprolaktonu (kapitola 4.2). Tato část práce popisuje také mechanismus, kinetiku a termodynamiku studované polymerace. Kapitola 4.3 pak porovnává *in-situ* polymeraci a míchání v tavenině jako dvě metody přípravy polykaprolaktonových nanokompozitů a popisuje účinek nanoplniv na mechanické, tepelné a bariérové vlastnosti nanokompozitů. Vliv alternativních (antibakteriálních) vrstevnatých podvojných hydroxidů na bázi Zn^{2+}/Al^{3+} modifikovaných iontovou kapalinou na aplikační (bariérové, baktericidní) vlastnosti nanokompozitů je popsán v kapitole 4.4, přičemž byla také hodnocena biologická odbouratelnost těchto nanokompozitů.

Bylo prokázáno, že *in-situ* mikrovlnná polymerace za otevření kruhu ε-kaprolaktonu za přítomnosti vrstevnatých podvojných hydroxidů modifikovaných iontovou kapalinou představuje efektivní způsob přípravy biologicky rozložitelných nanokompozitů na bázi polykaprolaktonu, které mohou nalézt využití např. jako aktivní obalové materiály.

Abbreviations

1% IL-ZnONPs	Polycaprolactone nanocomposite film prepared by microwave-assisted *in-situ* ring opening polymerization of ε-caprolactone with 1 wt.% of zinc oxide nanoparticles functionalized with ionic liquid
1% ZnONPs	Polycaprolactone nanocomposite film prepared by microwave-assisted *in-situ* ring opening polymerization of ε-caprolactone with 1 wt.% of zinc oxide nanoparticles
2% IL-ZnONPs	Polycaprolactone nanocomposite film prepared by microwave-assisted *in-situ* ring opening polymerization of ε-caprolactone with 2 wt.% of zinc oxide nanoparticles functionalized with ionic liquid
2% ZnONPs	Polycaprolactone nanocomposite film prepared by microwave-assisted *in-situ* ring opening polymerization of ε-caprolactone with 2 wt.% of zinc oxide nanoparticles
3% IL-ZnONPs	Polycaprolactone nanocomposite film prepared by microwave-assisted *in-situ* ring opening polymerization of ε-caprolactone with 3 wt.% of zinc oxide nanoparticles functionalized with ionic liquid
3% ZnONPs	Polycaprolactone nanocomposite film prepared by microwave-assisted *in-situ* ring opening polymerization of ε-caprolactone with 3 wt.% of zinc oxide nanoparticles
4% IL-ZnONPs	Polycaprolactone nanocomposite film prepared by microwave-assisted *in-situ* ring opening polymerization of ε-caprolactone with 4 wt.% of zinc oxide nanoparticles functionalized with ionic liquid
εCL	ε-caprolactone
AE	Anion exchange
AEC	Anion exchange capacity
C-Ca/Al	Calcinated Ca^{2+}/Al^{3+} layered double hydroxides
C-Ca/Al-D	Calcinated Ca^{2+}/Al^{3+} layered double hydroxides modified with trihexyltetradecylphosphonium decanoate
C-LDH	Calcinated layered double hydroxides
Ca/Al	Ca^{2+}/Al^{3+} layered double hydroxides (hydrated)
Ca/Al-D	Ca^{2+}/Al^{3+} layered double hydroxides (hydrated) modified with trihexyltetradecylphosphonium decanoate
CH	Conventional heating
DSC	Differential scanning calorimetry
FTIR	Fourier-transform infrared spectroscopy
GPC	Gel permeation chromatography
IL-D	Trihexyltetradecylphosphonium decanoate
IL-LDH	Layered double hydroxides functionalized with ionic liquid
IL-ZnONPs	Zinc oxide nanoparticles (calcinated Zn^{2+}/Al^{3+} layered double hydroxides) functionalized with trihexyltetradecylphosphonium decanoate
IL(s)	Ionic liquid(s)
Imim	Imidazolium
LDH	Layered double hydroxides
MALDI-TOF MS	Matrix-assisted laser desorption/ionization time-of-flight mass spectrometry
MB	Melt blending
MB-PCL	Neat PCL film
MB-PCL+C-Ca/Al	Polycaprolactone nanocomposite film prepared by melt-blending with 1 wt.% of calcinated Ca^{2+}/Al^{3+} layered double hydroxides
MB-PCL+C-Ca/Al-D	Polycaprolactone nanocomposite film prepared by melt-blending with 1 wt.% of calcinated Ca^{2+}/Al^{3+} layered double hydroxides modified with trihexyltetradecylphosphonium decanoate
MMO	Mixed metal oxides
MW	Microwave
NPs	Nanoparticles
PBAT	Poly(butylene adipate-*co*-terephthalate)
PBS	Poly(butylene succinate)
PCL	Polycaprolactone

PE	Polyethylene
PET	Poly(ethylene terephthalate)
PLA	Polylactide
PP	Polypropylene
ROP	Ring opening polymerization
ROP-PCL	Polycaprolactone prepared under microwave irradiation
ROP-PCL+C-Ca/Al	Polycaprolactone nanocomposite film prepared by microwave-assisted *in-situ* ring opening polymerization of ε-caprolactone with 1 wt.% of calcinated Ca^{2+}/Al^{3+} LDH
ROP-PCL+C-Ca/Al-D	Polycaprolactone nanocomposite film prepared by microwave-assisted *in-situ* ring opening polymerization of ε-caprolactone with 1 wt.% of calcinated Ca^{2+}/Al^{3+} LDH modified with trihexyltetradecylphosphonium decanoate
RTIL	Room temperature ionic liquid
SAXS	Small-angle X-ray scattering
TGA	Thermogravimetric analysis
WVP	Water vapor permeability
XPS	X-ray photoelectron spectroscopy
XRD	X-ray diffraction
XRF	X-ray fluorescence spectrometry
ZnONPs	zinc oxide nanoparticles; calcinated Zn^{2+}/Al^{3+} layered double hydroxides

Symbols

β	full width at half maximum of *hkl* reflection (Scherrer equation)
$\Delta G_a^{\ddagger}$	Gibbs free energy of activation
$\Delta H_a^{\ddagger}$	Enthalpy of activation
ΔH_m	Melting enthalpy
$\Delta S_a^{\ddagger}$	Entropy of activation
ε_{max}	Elongation at break
ε_r	Relative permittivity (dielectric constant)
λ	Incident X-ray wavelength
θ	Incident X-ray angle
θ_{H2O}	Water contact angle
σ_{max}	Tensile strength

A	Pre-exponential factor (Arrhenius equation)
C	Immediate monomer conversion
C_0	Initial monomer conversion
d	Basal spacing
$Đ$	Dispersity
$D_{(hkl)}$	Crystalline domain size
E	Young modulus
E_a	Activation energy
h	Planck constant
k	Kinetic rate constant; slope of kinetic equation of pseudo-first order reaction
K	Shape factor (Scherrer equation)
k_2	Kinetic rate constant of ring opening polymerization of ε-caprolactone catalyzed by ionic liquid
k_b	Boltzmann constant
$\overline{M}_n$	Number-average molecular weight
n	Diffraction order
P	Permeability coefficient
t	Reaction time
T_α	Alfa transition temperature
$T_{d5\%}$	Temperature at 5% sample weight loss
T_g	Glass transition temperature
T_m	Melting temperature
X_c	Crystallinity

1. Introduction

Nowadays, environmental concerns about growing polymer production and corresponding increase of plastic wastes have become an impulse for scientists and researchers in many fields related to the ecology, sustainable production and manufacturing to quest for greener alternatives of the currently applied materials and their fabrication processes. In the area of material technology, worth attention became polymer materials based on biodegradable matrix composed of linear polyesters (e.g. polylactide – PLA, polycaprolactone – PCL, poly(butylene succinate) - PBS, poly(butylene adipate-*co*-terephthalate) – PBAT, etc. [1]), known for their fast degradation under the influence of both biotic (presence and activity of microorganisms) and abiotic (e.g. temperature, humidity, oxygen and nutrients availability) factors [2]. Therefore, their use instead of conventional, non-biodegradable polymers (e.g. polyethylene – PE, polypropylene – PP, poly(ethylene terephthalate) – PET) is one step closer towards sustainability. From the view of manufacturing and chemical processing, environmentally benign technologies which enable to reduce process time and cut operating cost by lowering energy consumption are nowadays more and more adopted for synthesis of novel materials. As a response to this trend, microwave (MW) technology has begun to be frequently used in many applications (e.g. drying, dehydration, sterilization, etc.) due to its extreme efficiency and significant process acceleration [3,4].

1.1. Microwave-assisted ring opening polymerizations

Microwaves are part of the electromagnetic spectrum with frequencies of 300 MHz to 300 GHz corresponding to wavelengths of 1 m to 1 mm, respectively. The commercially available reactors using microwaves for heat generation operate at frequencies of 2.45 GHz or 900 MHz [5]. At these MW frequencies, the electromagnetic waves induce molecular rotations. When the material is exposed to MW irradiation, microwaves i) can be reflected from its surface when it is an electrical conductor (e.g. metals, graphite, etc.), ii) can penetrate it without absorption in the case of good insulators with good dielectric properties (e.g. quartz glass, porcelain, ceramics, etc.), iii) and can be absorbed by the lossy dielectrics (such as water, alcohol, etc.) [6]. The latter case is called dielectric (MW) heating and comprises absorption of MW energy and heat generation. Principle of dielectric heating consists in interacting with polar molecules (dipolar polarization) or charged particles (ions) and forcing them to realign with the electric field leading to rapid generation of thermal energy by rotations, friction or collisions of MW-excited molecules. Therefore, the nature of microwaves enables to use them as an energy source suitable for efficient and homogenous heating (also described as heating “inside out”) [7,8]. The conversion of electromagnetic energy into heat depends on the permittivity of the medium. Relative permittivity (dielectric constant, ε_r) specific for each compound is proportional to the interaction of the electric field with the medium, while dielectric loss is a measure for the

dissipation of this energy into heat. The ratio of dielectric loss to dielectric constant, also called the loss tangent, demonstrates the ability of any liquid to convert MW energy into heat [6].

So-called thermal/kinetic MW effects, such as volumetric heating (i.e. heating uniformly, at the same rate, in the entire volume of material), selective heating leading to localized overheating (formation of hot-spots due to direct absorption of MW irradiation) or ionic conduction are responsible for the enormous MW heating efficiency [7]. Due to the nature of MW heating, specific/non-thermal MW effects (decrease in the activation energy, increase in the pre-exponential factor due to enhanced collisions of molecules) may also have an influence on the process enhancement, however they have not been unequivocally explained as their investigation still remains a problematic issue [7].

MW-assisted processes have become also useful in the field of polymer chemistry due to many advantages of MW heating in comparison to conventional (conductive and convective) heating (CH). Firstly, MW heating enables to significantly reduce reaction time and increase the reaction yield [4,7–9]. Acceleration of the reaction rate is assigned to the decrease of activation energy of the polymerization reactions [8,10]. Additionally, extent of side reactions commonly occurring under CH is reduced by applying MW irradiation, which results in higher purity of synthesized materials and no necessity of conducting additional purification [7,11,12].

MW irradiation as the alternative, greener and more efficient heating method for the polymer synthesis has been applied for chain polymerizations: free radical polymerization [7,13], controlled radical polymerizations [14,15], ring opening metathesis polymerization [16] and ring opening polymerizations (ROP) of cyclic monomers (e.g. lactones [17], carbonates [18,19], oxazolines [20]). For these reactions, the application of MW heating is particularly advantageous, because no by-products, necessary to be removed during the course of polymerization, are formed.

Many recent studies reported strong lactone ROP rate dependence on the reaction temperature, thus the idea of using MW irradiation as more efficient heating method was found appropriate. The increasing MW power led to the much higher degree of ε-caprolactone (εCL) polymerization and higher monomer conversion [7,21,22] explained as a result of both thermal (depending on the MW power level [23]) and non-thermal MW effects [8]. Besides high efficiency of MW irradiation providing homogenous heating in whole reaction mixture, additional advantages, such as selective activation [24] and synergy between MW and enzymatic activity of enzyme-catalyzed ROP of lactones under MW, were found [9]. Exceptional MW effect on the rate of εCL ROP carried out using benzoic acid/tin(II) 2-ethylhexanoate as initiator/catalyst system was found to be a result of significant reduction of induction time in comparison to the ROP conducted under CH. Therefore, formation of initiating species proceeded much faster under MW irradiation and accelerated whole εCL ROP [24]. Liao et al. [25] reported highly efficient MW-assisted ROP of εCL in the presence of $Sn(Oct)_2$ or activated zinc powder, which led to

weight average molecular weight over 10^5 g·mol^{-1} with monomer conversion over 90% within 30 minutes. Nevertheless, the applied MW power (680 W) and the reaction temperature (210 °C) were inadequately too high, which increased energy consumption [23,25]. Kinetic and thermodynamic study of εCL ROP performed under MW irradiation in toluene reported by Yamada et al. [26] revealed that great enhancement of MW-assisted polymerization was mainly related to much larger entropic contribution resulting in significantly lower Gibbs free energy in comparison to CH.

Generally, cyclic esters (lactones), e.g. δ-valerolactone [27], εCL [27,28] or lactide (enantiomers or racemic mixture) [29–31], can undergo ROP via ionic (anionic or cationic) or coordination-insertion mechanisms [32] presented on the example of εCL in Fig. 1 and Fig. 2, respectively.

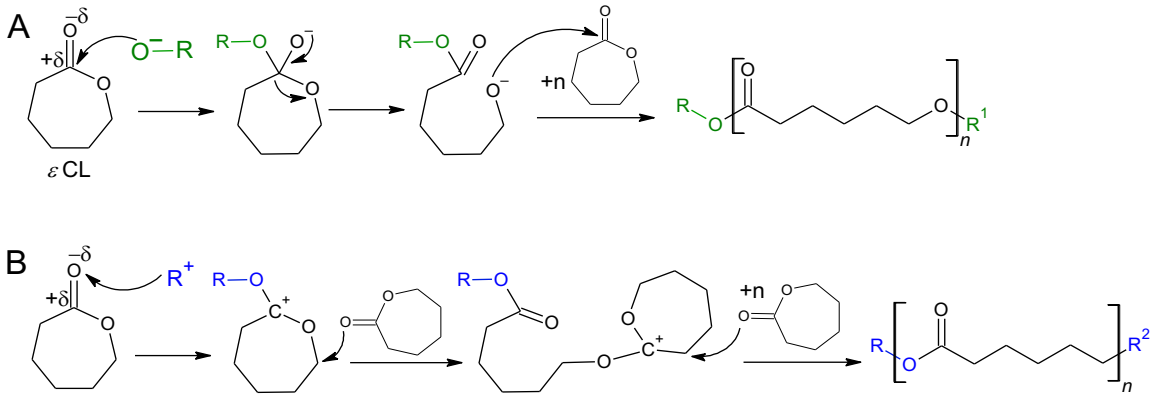

Fig. 1. Mechanisms of anionic (A) and cationic (B) ROP of εCL. Adapted from [32].

Anionic ROP of lactones (Fig. 1. A) is initiated via nucleophilic attack of alkoxides (RO^-) on the carbon atom (bearing partial positive charge) of carbonyl group followed by the cleavage of acyl-oxygen bond and results in opening of lactone ring and relocation of negative charge onto oxygen atom initially forming lactone ring. Oxyanion active center formed in the initiation step subsequently attacks carbonyl carbon atom of the next monomer molecule and propagation proceeds ideally till complete monomer conversion reflecting the living character of anionic ROP, which assumes no chain transfer and termination steps. Nevertheless, worth mentioning is that at later stage of lactone ROP, when the polymerizing chains are long enough and the viscosity of reactive system significantly increases with time, the chain transfer side reactions such as back-biting (intramolecular transesterification) leading to formation of cyclic (oligomeric) structures may occur [32]. This phenomenon results in bimodal distribution of final polymer and thus higher dispersity [33]. To avoid cyclization of propagating polyester chain, initiator reactivity can be tuned towards more favorable alkoxide attack on the monomer carbonyl group than on the oligomer/polymer ester group. This can be achieved by the electronic or steric effects of the substituents (-R). The first one is related to the substituent-induced changes in the electronic

structure (e.g. electron density) of the initiator molecule, whereas the latter rests on the applying substituents/ligands, which are sterically hindered. The reactivity of such initiator is reduced whereas its selectivity is improved [32].

Cationic ROP of lactones can be initiated by alkylating (Fig. 1. B) or acylating agents, Lewis bases or protonic acids [33,34]. If the alkylating agent is used, cation attacks the oxygen atom of carbonyl group resulting in positive charge transfer onto neighboring carbon atom. Such species subsequently react with another monomer molecule resulting in alkyl-oxygen bond cleavage, opening lactone ring and transfer of positive charge on the carbonyl carbon atom of the attached monomer molecule. Propagation proceeds further between newly formed carbocation and carbonyl oxygen atom of monomer analogically to this step [34].

In order to polymerize lactones via coordination-insertion mechanism (Fig. 2), the specific organometallic catalyst L_m-M-Nu (e.g. tin(II) 2-ethylhexanoate – $Sn(Oct)_2$, aluminum isopropoxide, zinc lactate, metal (Zn, Co, Cu) octoate [33,35,36]) and alcohol (if non-alkoxide catalyst is used) are needed. Initiator is formed by the alcoholysis of metal-nucleophile (M-Nu) bond, which results in generation of alkoxide species (L_m-M-OR). These species directly initiate ROP via coordination-insertion to the carbonyl group of the monomer molecule followed by opening of lactone ring and formation of L_m-M-O-$(CH_2)_5$-CO-O-R species (in the case of εCL ROP), which are able to coordinate next monomer molecules so the propagation proceeds [34].

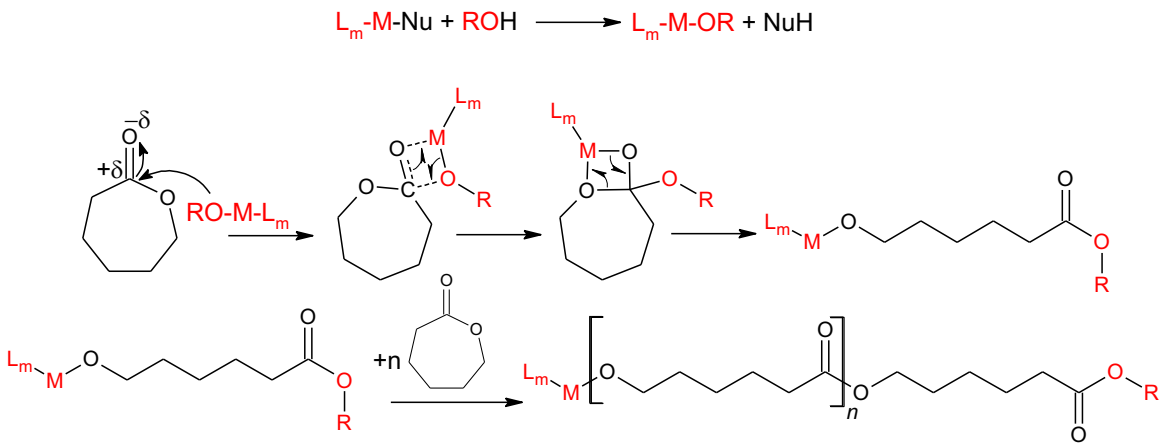

Fig. 2. Coordination-insertion mechanism of εCL ROP. Adapted from [34].

The coordination-insertion mechanism promoted by the organometallic catalysts is by far the preferred synthesis of linear aliphatic polyesters due to its mild and solvent-free (bulk) conditions, a high yield and possibility to synthesize polymers with targeted macromolecular parameters (polymer structure, molecular weight, dispersity, etc.) [34]. However, the catalyst toxicity and contamination of the resulting product by metal residues are serious concerns limiting the use of produced polyesters in many applications requiring non-toxicity and biodegradation (medical products, biodegradable packaging for food industry, agricultural films, etc.). Therefore,

recent effort has been focused on developing metal-free organic species [37,38] with high efficiency to initiate/catalyze ROP which can be the green alternatives to the traditional metal-based catalysts. So far the major drawbacks for these new organo-catalytic ROP still to be overcome are long reaction time [39–41], low monomer conversion [39,40] and molecular weight [6,27,42], high polymer dispersity [39,40,43] as well as the necessity to use harmful organic solvents [39,42].

1.2. *In-situ* preparation of polyester nanocomposites under microwave irradiation

Inferior properties (mechanical, thermal, barrier) of the neat aliphatic polyesters (PCL, PLA etc.), which limit their application for i.e. food packaging, can be compensated via incorporation of nanoparticles (NPs) into polymer matrices [3]. *In-situ* synthesis under MW irradiation can lead to efficient and fast preparation of nanocomposites with well-dispersed NPs owing to low initial viscosity of reaction mixture and thus enhanced NPs delamination in polymer matrix [44]. In addition, MW-induced acceleration of ROP is advantageous since NPs precipitation can be easily avoided due to much shorter reaction time [3].

MW-assisted *in-situ* (bulk) ROP of lactones performed in the presence of various NPs, such as boron nitride [3,45], layered silicates (e.g. montmorillonite) [12], silica, graphene or hydroxyapatite [44], has been currently investigated. Among the various types of NPs, 2D layered double hydroxides (LDH) were found suitable for manufacturing of the polyester (e.g. PET [46], [47], polyhydroxyalkanoates [48], PLA [49] or PCL [50]) nanocomposites with the improved mechanical and barrier properties in comparison to the neat polymers. However, the polyester-LDH nanocomposites were usually prepared via melt [48] or solution [49,50] intercalation. The *in-situ* preparation of these nanocomposites was carried out via polycondensation [51,52], while the *in-situ* ROP of lactones in the presence of LDH neither under CH nor MW has been rarely studied [53,54]. Moreover, due to a low LDH toxicity and ability to be intercalated by various compounds, LDH seem to be promising candidates for new nanofillers for biodegradable polyesters possessing multifunctional properties, e.g. active (antimicrobial) packaging [52].

1.3. Layered double hydroxides: structure and properties

LDH bearing general formula $[M^{2+}_{1-x}M^{3+}_{x}(OH)_2]^{x+}(A^{n-})_{x/n}\cdot zH_2O$ (M^{2+}, M^{3+} and A^{n-} stand for divalent metal cation, trivalent metal cation and interlayer anion, respectively) represent a group of 2D hexagonal anionic clay NPs, which are naturally occurred as hydrotalcite mineral or can be synthesized via e.g. co-precipitation, sol-gel or hydrothermal route [55]. Molar ratio of divalent/trivalent cation (1-x)/x usually varies between 0.2 to 0.33, thus M^{2+} cations are in majority. Both M^{2+} (e.g. Mg^{2+}, Ca^{2+}, Zn^{2+}) and M^{3+} (e.g. Al^{3+}, Cr^{3+}, Fe^{3+}) together with hydroxyl groups (6 per each cation) form positively-charged brucite-like layers (0.48 nm thickness) composed of octahedral units (Fig. 3) [55–57]. Inorganic anions A^{n-} (e.g. CO_3^{2-}, NO_3^-, Cl^-) placed

with water in the interlayer space stabilize LDH structure due to strong interactions of hydroxyl groups homogenously distributed over each LDH layer and interlayer anions/water [55,56]. Interlayer spacing (also called basal spacing) determines the distance between the single LDH layers and depends on the type of intercalated anions and the content of interlayer water [55].

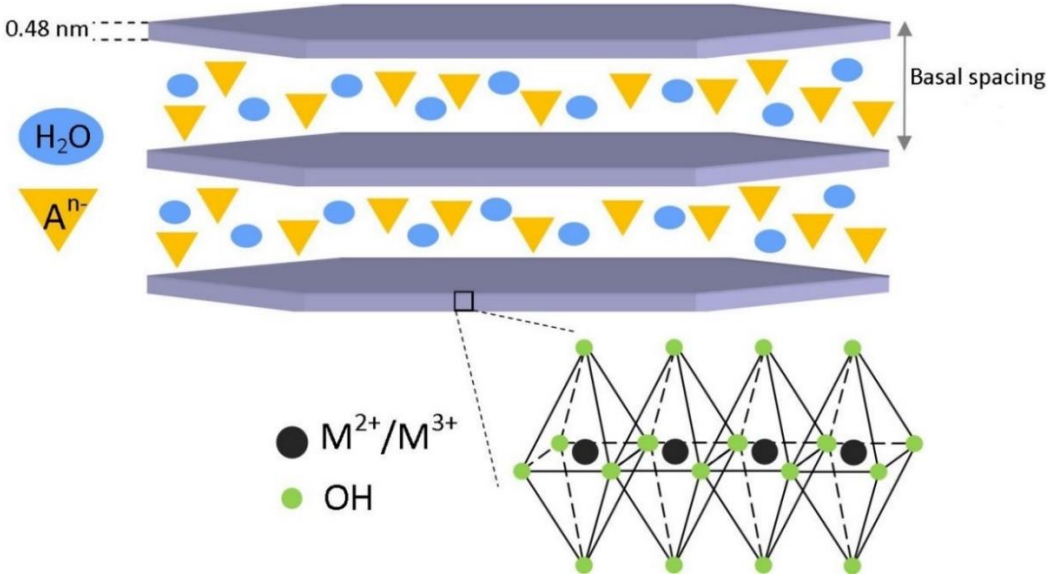

Fig. 3. Schematic presentation of the LDH structure. Adapted from [56].

LDH exhibit unique properties, such as remarkable thermal and chemical stability, high surface area (surface/volume ratio), high sorption and loading capacity due to high anion exchange capacity (AEC). Additionally, LDH are low-cost, non-toxic, biocompatible nanomaterials [55,56], widely applied in sorption, water treatment, as nanocomposite fillers, additives in food packaging etc. [56,57].

Calcination of LDH (thermal treatment at elevated temperature usually above 500 ^{o}C), explained as activation in terms of catalytic activity, leads to formation of mixed metal oxides (denoted as MMO or C-LDH – calcinated LDH) with higher surface area than that of hydrated LDH. C-LDH exhibit improved thermal stability, higher sorption capacity and enhanced catalytic efficiency due to the presence of easily accessible metal atoms [56,58].

Although the use of LDH as heterogeneous (solid) catalysts for e.g. transesterification [59], Michael addition or epoxidation [60] was reported, it was found that inorganic/organic modification (also called functionalization) of LDH significantly increased the catalytic efficiency of resulting LDH.

1.3.1. Modification routes for layered double hydroxides

Modification of LDH structure can be performed via surface functionalization (usually based on adsorption) or anion exchange (AE) reaction, during which the initially intercalated small anions with low binding energy are exchanged with the larger (organic) anions having

higher binding energy [55,61]. The introduction of bulky anions into the interlayer space results in extension of the basal spacing, which enhances penetration of molecules between LDH layers and further supports LDH delamination and exfoliation (separation of LDH into single layers homogenously dispersed in a selected medium) [55]. Ability of the host anions to exchange the original ones depends on charge and size of an anion. The improved exchangeability was observed for the host anions with higher charge and smaller radius than those of the anions initially present in the interlayer. Additionally, solvent type and pH also strongly affect the AE process [56].

It has been recently demonstrated that ionic liquids (ILs) with highly variable chemical structures can be advantageously used for LDH modification leading to preparation of IL-functionalized LDH (IL-LDH). Thus modified NPs act as curing agents for epoxy resin [62], adsorbents [63–67], (photo)catalysts [63,68], solid electrolytes for batteries [69] or components for electrochemical determination of transition metals [70].

1.3.2. Layered double hydroxides as catalyst support

LDH themselves were found to be a versatile materials for preparation of interfacial, highly efficient catalysts bearing active sites owing to their i) tunable chemical (types and ratio of metal cations in the LDH layers) and crystalline (exfoliation induced by increasing basal spacing) structure, ii) so-called anchoring effect related to the homogenously distributed OH groups which can bond metal atoms, iii) presence of exchangeable interlayer anions (introduction of catalytic species between LDH layers), iv) memory effect (calcinated Mg^{2+}/Al^{3+} LDH reconstruct crystalline structure of hydrated LDH in water) and v) ability to confine host molecules on the surface (external confinement) or between layers (internal confinement) [61]. The catalytic reaction usually proceeds on a thin layer on the LDH surface. Therefore, LDH were applied as solid supports for various catalytic species achieving the same catalytic efficiency as non-immobilized catalyst, but at much lower concentration [55]. Thus, the intercalation of catalytic active species between LDH layers leads to efficient, easily separable catalytic system with larger number of stable interfacial sites [61]. Moreover, the catalyst immobilization on LDH support enables to better control course of the reaction, e.g. in case of chain polymerization it leads to lower polymer dispersity [7].

Kredatusová et al. [54] observed the MW-induced acceleration of the *in-situ* ROP of εCL in the presence of IL immobilized on LDH. However, possible initiating/catalyzing effect of the IL-LDH was not fully explored.

The above-mentioned benefits of LDH together with the IL ability to catalyze many processes (including ROP) were the strong motivation for this thesis, in which the catalytic role of LDH with the immobilized IL (IL-LDH) for MW-assisted ROP of lactones will be investigated. This approach combines a concept of the IL-LDH catalysis together with the MW-accelerated

ROP due to MW-absorbing capability of IL. No further experiments, e.g. kinetic/thermodynamic study of the MW-assisted, IL-LDH catalyzed εCL ROP or investigation of the IL-LDH effect on the final polymer/nanocomposite material properties (mechanical, thermal, barrier etc.), have been published and therefore, they will be the subject of this thesis.

1.4. Ionic liquids in polymer synthesis

ILs are classified as organic salts bearing a large organic cation (Fig. 4. A-C) and an organic/inorganic anion (Fig. 4. D). The most of ILs are liquid at room temperature (RTIL – room temperature ionic liquid) [71–73]. ILs exhibit unique, easily-tunable and structure-related (depending on the type of cation and anion) properties, such as good chemical and thermal stability, low vapor pressure (low volatility), high conductivity and dissolving ability for various organic/inorganic compounds. Therefore, ILs are considered as versatile solvents for many syntheses, i.e. polymer synthesis, or suitable extraction media [71,74–76]. The above-mentioned properties are related to i) the chemical structure of ILs and ii) the interactions present in the bulk ILs, mainly the electrostatic cation-anion interactions and the short-range interactions of non-polar chains (marked as R on Fig. 4. A-C). Owing to this phenomenon, ILs form heterogeneous (three-dimensionally structured) domains affecting their reactivity, which can be also influenced by the direct interactions of IL with reactive species present in polymerization system [71].

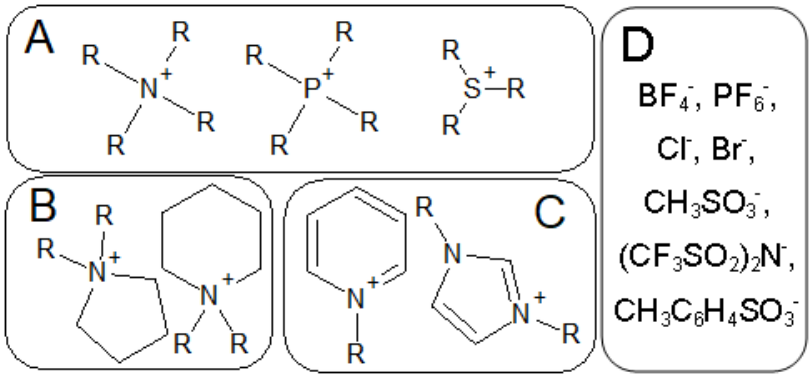

Fig. 4. Structures of IL cations (A: ammonium, phosphonium or sulfonium cations; B: cyclic pyrrolidinium and piperidinium cations; C: aromatic pyridinium and imidazolium cations) and frequently used anions (D). Adapted from [73].

1.4.1. Ionic liquids as polymerization solvents under microwave irradiation

In case of low MW-absorbing reaction systems, the addition of non-reactive polar molecules (e.g. as solvents) leads to an increase of reaction rate due to the enhanced MW absorption by the whole reaction mixture. ILs are suitable additives for MW-assisted polymerizations owing to their remarkable heating efficiency, which results from their ionic character. Their addition enables selective heating, better control of reaction temperature and time, higher molecular weight and lower polymer dispersity [4,7,19]. Another advantage of using

IL as solvents for MW-assisted polymerizations is the possibility to conduct the reaction at higher temperature, which usually exceeds boiling point of conventional organic solvents [7].

Although lactones are polar molecules easily absorbing MW irradiation [4], even small addition of IL into εCL further enhanced the MW absorption of the reaction mixture [8,24,77,78]. While the lack of IL can lead to significantly limited progress of ROP, in contrast a relatively high content (10-20 wt.%) of 1-butyl-3-methylimidazolium tetrafluoroborate negatively increased the dispersity of final PCL [7,78]. Therefore, finding an optimum IL content, which enhances MW absorption, but does not cause unwanted overheating (possible thermal degradation) or decreasing of polymer dispersity, is highly desirable.

1.4.2. Ionic liquids as interfacial agents

ILs were found to be efficient compatibilizers improving miscibility of polymer blends, e.g. PLA-PBAT [79–81], PLA-poly(ethylene-vinyl acetate) [82], PBS-starch [83], styrene-butadiene rubber/aramid fibers [84] as well as their inorganic hybrids with e.g. talc [85] or carbon nanotubes [86]. Application of ILs for preparation of polymer blends or (nano)composites resulted in significantly improved mechanical [80–87] and thermal [83,85] properties of final materials. Owing to their ionic character, the enhanced electrical conductivity of IL-modified carbon nanotubes was also reported [86]. Additionally, ILs acted as plasticizing agents [87] or flame retardants (in case of phosphonium-based ILs) [81]. Recent studies have also reported the enhanced compatibility between polymer matrix and IL-modified inorganic fillers e.g. halloysite [87], silica [88] or LDH [89–91].

1.4.3. Ionic liquids as catalysts

Although catalytic effect of ILs (mostly imidazolium ILs) in various organic syntheses (e.g. Michael addition [92], oxidation, hydrogenation, cycloaddition [93]) and polymerization reactions (e.g. radical polymerization of acrylates [94,95], ROP of epoxy rings [96] or polycondensation [97]) has been reported, ILs are predominantly applied as polymerization media for MW-assisted syntheses.

Currently, ILs are applied for biphasic catalytic systems in which IL dissolves and immobilizes the catalyst (usually metal/metal complex together forming one phase), whereas reagents form second phase. This approach enables easier catalyst separation and its recycling. On the contrary, leaching of the catalyst from IL into reaction medium, possibility of water sorption by IL resulting in deactivation of catalyst and necessity of use relatively large amount of ILs are the main disadvantages of IL biphasic catalytic systems [98]. These disadvantages can be overcome by IL immobilization on a solid support.

Recent studies on εCL ROP showed a catalytic effect of free [99] or immobilized imidazolium (Imim) ILs [100] emphasizing their versatility and non-metal structure. Homogenous

Imim ILs catalysis conducted in bulk revealed that εCL ROP exhibited a living character. The ROP activation was related to the strength of hydrogen donor in Imim cation depending on the type of counterion and the monomer-IL interactions (hydrogen bonding) [99]. Cruz et al. [100] combined the Imim IL immobilized on solid support (silica) with a conventional catalyst (titanium isopropoxide). The results indicated that the content of both titanium isopropoxide and IL had influence on the overall catalytic efficiency and led up to 100% monomer conversion within 2 h and low PCL dispersity (1.13).

The catalytic potential of ILs bearing other cations than Imim for ROP of lactones has not been reported in the literature so far.

2. Aims of the thesis

The aim of this thesis is to study the MW-assisted ROP of εCL in the presence of LDH as a green synthetic route for production of biodegradable nanocomposites with application potential in sustainable packaging.

Particular aims have been specified:

- synthesis and characterization of different types of LDH via co-precipitation method,
- modification of LDH with various ILs via AE reaction or surface functionalization and their characterization,
- study of the IL-modified and non-modified LDH role in the εCL ROP under MW irradiation,
- application of the modified and non-modified LDH for the preparation of PCL nanocomposites: comparison of MW-assisted *in-situ* synthesis and melt-blending (MB),
- study of the effect of IL and IL-LDH on the mechanical, thermal, barrier, antibacterial properties and biodegradation rate of prepared PCL nanocomposites.

3. Experimental part

This doctoral thesis has arisen from a kind cooperation with my colleagues from Institute of Macromolecular Chemistry, CAS (IMC), Institute of Inorganic Chemistry, CAS (IIC) and Faculty of Food and Biochemical Technology, University of Chemistry and Technology in Prague (UCT).

In experimental part of my PhD study, I have synthesized Mg^{2+}/Al^{3+} and Ca^{2+}/Al^{3+} LDH via co-precipitation method and functionalized them with various ILs via AE reaction (subsections 4.1 and 4.2.1). I have also conducted the surface modification of calcinated forms of LDH based on calcium (subsection 4.2.1) and zinc (subsection 4.4; prepared by Ing. Petra Ecorchard, Ph.D. from IIC) with the selected IL. My further responsibilities have rested on conducting εCL ROP under MW irradiation in the presence of various LDH (subsection 4.2.2); on the basis of these experiments, I have performed a kinetic/thermodynamic study of the selected model reaction (subsection 4.2.2) and proposed the mechanism of IL-catalyzed polymerization (subsection 4.2.3). Further, I have prepared PCL-LDH nanocomposites via two methods (subsections 4.3 and 4.4): the MW-assisted *in-situ* polymerization and the melt blending and processed them to receive thin PCL-LDH films suitable for application-related testing (e.g. barrier properties).

In order to characterize the synthesized LDH and PCL-LDH nanocomposites, I have performed experiments, analyzed (unless otherwise stated) and correlated data obtained from the various methods listed below with brief description of their use:

Fourier-transform infrared spectroscopy (FTIR): characterization of LDH chemical structure, verification of LDH modification with ILs (presence of adsorbed and intercalated IL in the IL-LDH).

X-ray diffraction (XRD): crystallographic characterization of LDH (according to Bragg's law described in the subsection 4.1) and PCL-LDH nanocomposites; verification of LDH modification with ILs (presence of the IL species intercalated between IL-LDH galleries); calculation of PCL crystallite sizes in PCL-LDH nanocomposites (according to Scherrer equation described in the subsection 4.3). XRD patterns were measured by Magdalena Konefał, Ph.D. (IMC).

Thermogravimetric analysis (TGA): thermal stability of LDH and PCL-LDH nanocomposites; weight content of adsorbed/intercalated water in LDH; weight content of IL in calcinated LDH (C-LDH) modified with IL.

Scanning electron microscopy (SEM) and *transmission electron microscopy* (TEM): morphology of LDH. Microphotographs were taken by Ing. Ewa Pavlova, Ph.D. (IMC).

X-ray photoelectron spectrometry (XPS): presence of surface-bonded IL in IL-LDH. Measurements and analyses were performed by RNDr. Jan Svoboda, Ph.D. (IMC).

X-ray fluorescence spectrometry (XRF) and *elemental analysis*: calcium, aluminum (XRF) and carbon, nitrogen (elemental analysis) weight contents in LDH for the determination of LDH chemical formulae; estimation of IL weight content in the IL-intercalated LDH (combined with TGA results). Weight contents of the selected elements were determined by RNDr. Olga Trhliková, Ph.D. (IMC).

Small-angle X-ray scattering (SAXS): course of LDH delamination process. SAXS profiles were measured and analyzed by Magdalena Konefał, Ph.D. (IMC).

Gel permeation chromatography (GPC): determination of number-average molecular weight ($\bar{M}_n$) and dispersity ($Đ$) of synthesized oligomers/polymers; calculation of monomer conversion.

Matrix-assisted laser desorption/ionization time-of-flight mass spectroscopy (MALDI-TOF MS): course of polymerization; end-group analysis of reaction products (determination of initiating species and polymer structures). MALDI-TOF mass spectra were measured by Ing. Zuzana Walterová (IMC).

Dynamic mechanical thermal analysis (DMTA): alfa transition temperature (T_α) of PCL-LDH nanocomposites. DMTA measurements were performed by Ing. Jiří Hodan (IMC).

Differential scanning calorimetry (DSC): glass transition temperature (T_g), melting temperature (T_m) and crystallinity (X_c) of PCL-LDH nanocomposites.

Contact angle measurement: effect of IL-modified and non-modified LDH on the wettability of PCL-LDH nanocomposites.

Tensile test: mechanical properties (Young modulus E, tensile strength σ_{max} and elongation at break ε_{max}) of PCL-LDH nanocomposites. Tensile measurements were performed by Ing. Jiří Hodan (IMC).

Barrier properties: permeability of oxygen, carbon dioxide and water vapor for PCL-LDH nanocomposites. Measurements and analyses were performed by Ing. Jakub Peter, Ph.D. (IMC).

Antibacterial activity test: antibacterial activity of PCL-LDH nanocomposites. Measurement, data curation and analyses were performed by doc. Ing. Martin Halecký, Ph.D. (UCT).

Accelerated biodegradation test: biodegradability of PCL-LDH nanocomposites with selected microorganisms was performed by doc. Ing. Martin Halecký, Ph.D. (UCT).

Specific instruments, equipment and syntheses/measurement conditions were described in details in relevant publications listed on the page 54 (appendices to this thesis).

4. Results and Discussion

4.1. Modification of layered double hydroxides with ionic liquids

Appendix 1: *Ionic Liquids as Delaminating Agents of Layered Double Hydroxide during In-Situ Synthesis of Poly (Butylene Adipate-co-Terephthalate) Nanocomposites*

Firstly, IL-LDH based on commonly used Mg^{2+} and Al^{3+} cations as non-toxic IL support were prepared via direct co-precipitation method in the presence of IL dissolved in the organic solvent (depending on the IL type). The main advantage of this method is fast one-step preparation of LDH modified with selected IL. Herein, phosphonium ILs bearing various anions, such as bis(2,4,4-trimethylpenthyl)phosphinate, decanoate, and bis(2-ethylhexyl)phosphate combined with trihexyltetradecylphosphonium cation were used (Fig. 5).

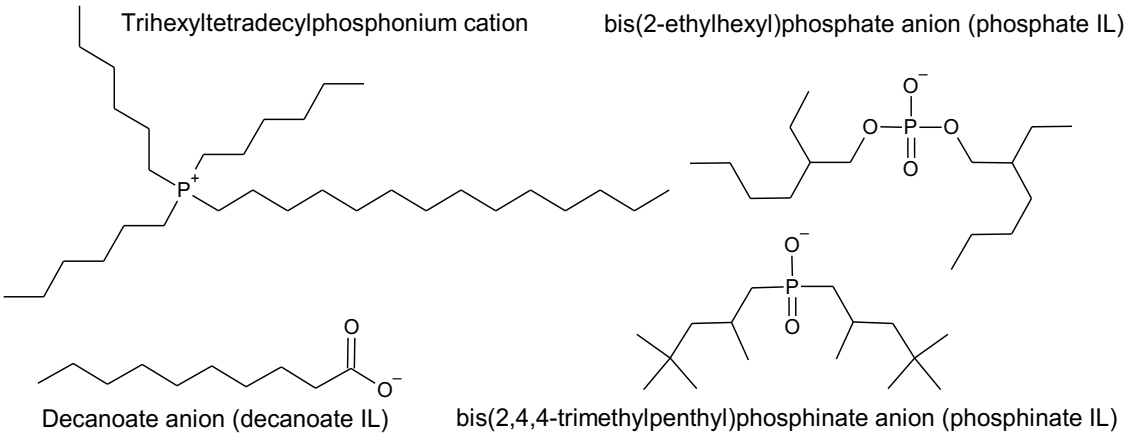

Fig. 5. Structures of ILs used for LDH modification.

Successful immobilization of IL in each IL-LDH was proved on the basis of their FTIR spectra (Fig. 6. A, b-d), which indicate the presence of organic species related to C-H stretching vibrations in hydrocarbon chain (2850-2960 cm^{-1}). The other characteristic vibrations reflecting the presence of IL anions (e.g. POO^- at ca. 1021 cm^{-1} and 1131 cm^{-1}, COO^- at ca. 1551 cm^{-1} or $POCH_2$ at the range of 1351-1021 cm^{-1}) were also detected. FTIR spectra of IL-LDH and pristine LDH reveal also the presence of inorganic carbonate anions at 1360 cm^{-1}, which are known as the most stable in the LDH interlayer due to the highest affinity of CO_3^{2-} to LDH and thus, their presence in LDH structure is almost inevitable.

In order to determine whether IL was adsorbed on LDH surface or intercalated between LDH layers, crystalline structure of all prepared IL-LDH was studied using XRD (Fig. 6. B). The XRD pattern of non-modified Mg^{2+}/Al^{3+} LDH (Fig. 6. B. a) shows characteristic reflections at 11.53° (003), 23.38° (006) and 35.28° (009), while the XRD patterns of IL-LDH (Fig. 6. B. c-d) indicate significant shift of the (003) reflection to lower 2θ values: 3.39°, 3.05° and 2.19° for LDH modified with phosphate IL, decanoate IL and phosphinate IL, respectively. Worth mentioning is that the (003) reflection corresponds to the basal spacing of LDH, thus reflects the distance

between LDH layers, which is mostly affected by the type of intercalated anions. The basal spacing *d* was calculated according to the Bragg's law: $n\lambda=2dsin\theta$, where *n* is diffraction order, whereas λ and θ correspond to wavelength and angle of an incident X-ray.

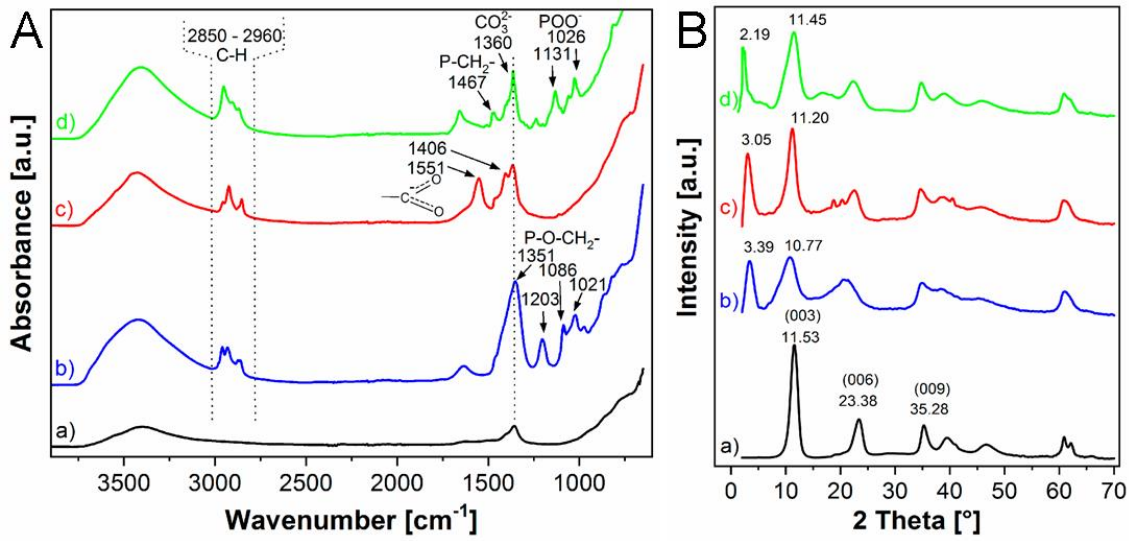

Fig. 6. FTIR spectra (A) and XRD patterns (B) of a) pristine Mg^{2+}/Al^{3+} LDH and Mg^{2+}/Al^{3+} LDH modified with b) phosphate IL, c) decanoate IL and d) phosphinate IL. Adapted from [101].

The *d* values for all IL-LDH were significantly extended (2.6, 2.9 and 4.0 nm for LDH modified with phosphate IL, decanoate IL and phosphinate IL, respectively) in comparison to that of pristine LDH (0.77 nm) confirming intercalation of LDH with IL anions regardless IL type. Nevertheless, the broad reflections on the IL-LDH patterns at 10.77° (phosphate-modified LDH), 11.20° (decanoate-modified LDH) and 11.45° (phosphinate-modified LDH) indicate formation of the second non-intercalated LDH. Another explanation could be alternative orientation of phosphate, decanoate and phosphinate anions between LDH layers, since all IL anions have flexible hydrocarbon chains.

TGA (Fig. 7) of all LDH based on Mg^{2+} and Al^{3+} reveals two separated degradation steps at 50-250 °C and 250-500 °C. The first step corresponds to the adsorbed/intercalated water in all synthesized LDH, whereas the second step is related to the decomposition of intercalated anions (both inorganic and organic) and dehydroxylation of LDH layers (removal of surface OH groups), which results in formation of MMO (MgO and Al_2O_3 in this particular case). The derivative TGA (DTG) curves of IL-LDH (on the bottom of Fig. 7) clearly show the degradation of organic IL species: at least two degradation maxima appeared for all IL-LDH, whereas only one maximum on the DTG curve of pristine LDH was observed (Fig. 7. black curve). Moreover, the total solid residues after TGA of each IL-LDH (ca. 45-50%) were much lower than those of the pristine LDH (ca. 57%), which enables to estimate the IL weight contents introduced into the LDH structure: 11.8%, 12.6% and 7.4% for LDH modified with phosphate IL, decanoate IL and phosphinate IL, respectively. However, the exact IL content and its localization in IL-LDH (ratio

of intercalated IL anions/adsorbed IL species) was impossible to be determined due to overlapping degradations of IL/inorganic (carbonate) anions and proceeding LDH dehydroxylation.

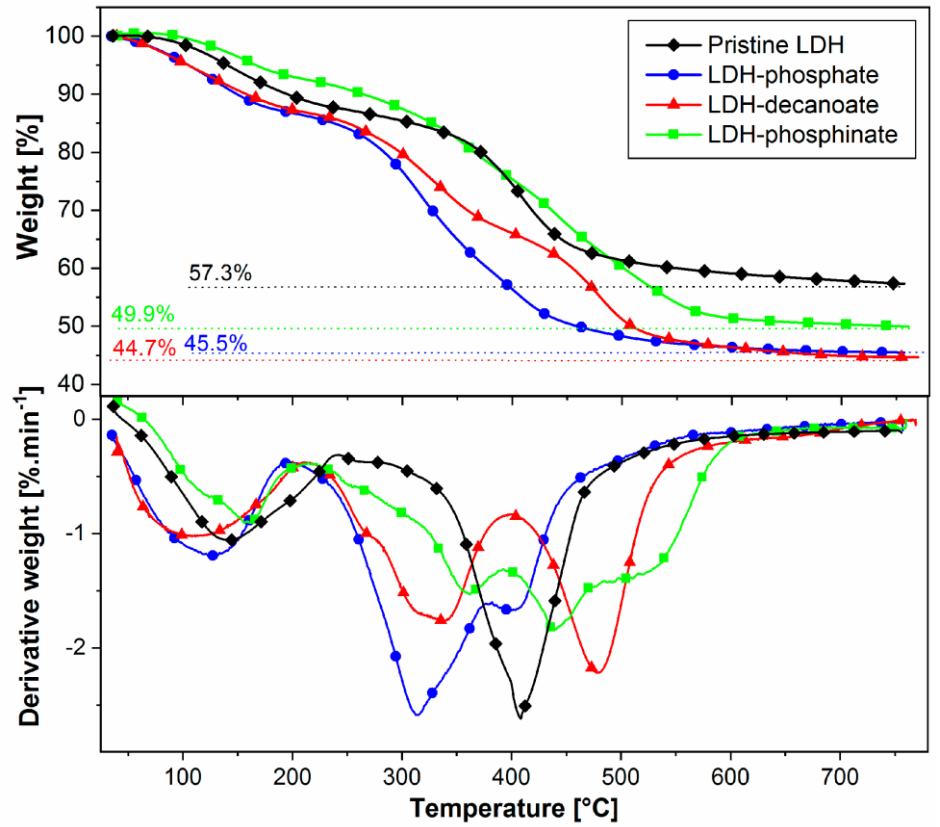

Fig. 7. TGA and DTG curves of pristine Mg^{2+}/Al^{3+} LDH and Mg^{2+}/Al^{3+} LDH modified with b) phosphate IL, c) decanoate IL and d) phosphinate IL. Adapted from [101].

Although the relatively fast and straightforward (one-step) co-precipitation of LDH based on Mg^{2+}/Al^{3+} in the presence of ILs led to successful immobilization of IL species between LDH galleries and on LDH surface, IL-LDH were inhomogeneous (partially IL-intercalated) and the IL amount was only roughly estimated. Therefore, we decided to design and synthesize another type of LDH, which would allow the preparation of fully IL-intercalated LDH with homogenous crystalline structure.

4.2. Initiating/catalytic layered double hydroxides-ionic liquid system for microwave-assisted ε-caprolactone ring opening polymerization

Appendix 2: *Ionic liquid-functionalized LDH as catalytic-initiating nanoparticles for microwave-activated ring opening polymerization of ε-caprolactones*

Preliminary experiments with a Ca^{2+}/Al^{3+} type of LDH indicated that they had larger basal spacing than Mg-based LDH in the pristine form, which enhanced their modification with IL via AE reaction. Moreover, Ca-based LDH revealed three nicely separated degradation steps

corresponding to i) a water removal, ii) the decomposition of interlayer anions and iii) the dehydroxylation, which enables to properly calculate the IL content. These factors made them attractive alternative to the Mg-based LDH for IL-LDH preparation.

4.2.1. Characterization of layered double hydroxides functionalized with ionic liquid

Two different types of non-modified Ca^{2+}/Al^{3+} LDH (hydrated Ca/Al) and its calcinated form (C-Ca/Al), were prepared to study the effect of surface OH groups on the course of εCL ROP. Both LDH were further modified with trihexyltetradecylphosphonium decanoate IL (IL-D) obtaining IL-modified forms: the hydrated Ca/Al-D and the calcinated C-Ca/Al-D. IL-D was chosen due to i) easy intercalation of decanoate anions into LDH structure, which led to the high IL content, and ii) its chemical similarity (linear hydrocarbon chain ended with carboxylic group) to PCL chain (subsection 4.1).

The crystalline structure of hydrated Ca/Al (strong OH band at 3500-3600 cm^{-1} on the Ca/Al FTIR spectrum, Fig. 8. B. a) studied using XRD (Fig. 8. A. a) corresponded to the typical crystallographic pattern of Ca^{2+}/Al^{3+} LDH with the (002), (004) and (006) reflections at 10.3°, 20.6° and 31.1°, respectively. In comparison to the pristine Mg^{2+}/Al^{3+} LDH (d=0.77 nm), basal spacing of Ca/Al was extended to 0.86 nm, which enhanced the subsequent AE reaction. The highly crystalline Ca/Al treated at 500 °C was transformed into C-Ca/Al, which consisted mainly of calcium carbonate and traces of MMO (herein $Ca(OH)_2$, Al_2O_3) - the XRD pattern of C-Ca/Al (the intensive reflection at 29.3° characteristic for $CaCO_3$, Fig. 8. A. b). The FITR spectrum of C-Ca/Al (Fig. 8. B. b) confirms complete removal of surface OH groups (no broad band around 3500 cm^{-1}) and significant decrease of water (no signal at 1640 cm^{-1}) after calcination.

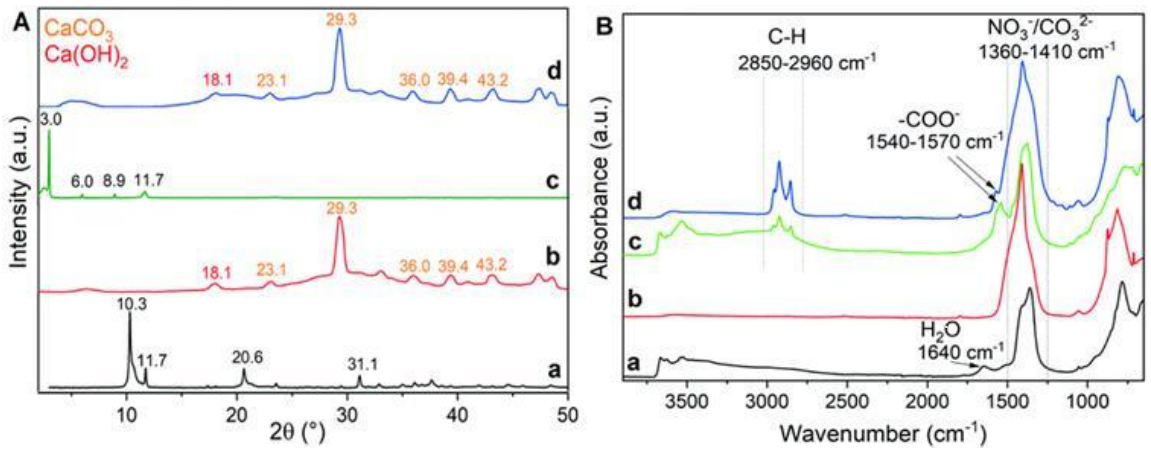

Fig. 8. XRD patterns (A) and FTIR spectra (B) of Ca-based LDH: a) Ca/Al, b) C-Ca/Al, c) Ca/Al-D and d) C-Ca/Al-D. Adapted from [102].

Worth mentioning is that the C-Ca/Al modification with IL took place only on the surface of NPs due to change in its crystalline structure in comparison to Ca/Al: well-organized layered structure of Ca/Al with intercalated anions collapsed after thermal treatment (calcination). Thus

no AE reaction was possible in C-Ca/Al due to lack of exchangeable anions. Therefore, possible location of IL-D varies with the type of LDH. In the case of Ca/Al-D, IL-D might be both intercalated (only decanoate anion) and adsorbed on its surface (whole IL), whereas in C-Ca/Al-D, IL-D can only be immobilized on the surface. Successful modification of Ca/Al and C-Ca/Al with IL-D was confirmed by the presence of C-H (2850-2960 cm^{-1}) and COO^- (1540-1570 cm^{-1}) bands on the corresponding FTIR spectra of Ca/Al-D and C-Ca/Al-D (Fig. 8. B. c-d) referring to the used IL. The XRD pattern of Ca/Al-D (Fig. 8. A. c) clearly indicates the intercalation of decanoate anion since all characteristic reflections were shifted to 3.0° (002), 6.0° (004) and 8.9° (006) and the corresponding basal spacing of Ca/Al-D was extended to 2.9 nm. Such unexpected *d* extension was a result of preferential formation of decanoate dimers between Ca/Al-D layers. The crystallographic pattern of C-Ca/Al-D (Fig. 8. A. d) remained unaffected by the introduction of IL-D immobilized on the C-Ca/Al-D surface.

In order to further confirm IL-D location in the prepared IL-LDH, XPS analysis of their surface was performed (Fig. 9. E). The surface modification of C-Ca/Al-D was confirmed by the signals corresponding to phosphorus of IL cation: the spin-split doublet with peaks P $2p_{3/2}$ and P $2p_{1/2}$ (Fig. 9. E, the middle spectrum). On the contrary, the spectrum of hydrated Ca/Al-D reveals no signal related to the phosphorus of IL cation (the bottom curve in Fig. 9. E), which indicates no presence of surface-bonded IL-D in this LDH. Thus, functionalization of Ca/Al-D proceeded only via the AE reaction (no IL-D was adsorbed on the Ca/Al-D surface) and the total organic fraction in Ca/Al-D corresponded to the interlayer decanoate anions.

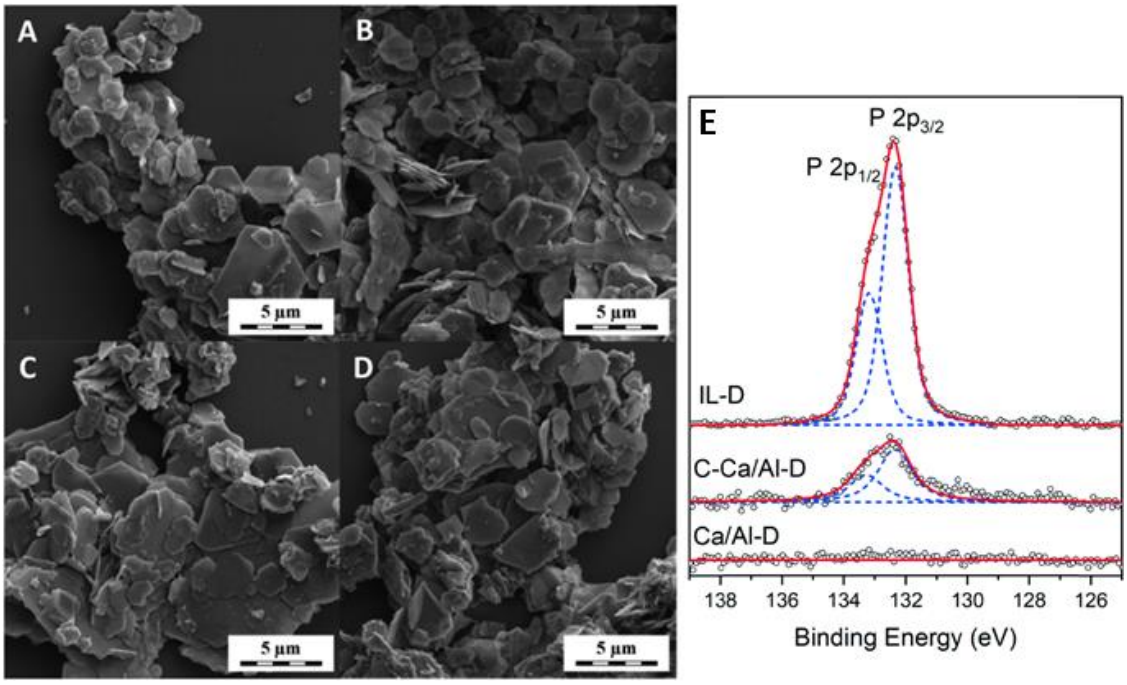

Fig. 9. SEM microphotographs of prepared LDH: A) Ca/Al, B) Ca/Al-D, C) C-Ca/Al and D) C-Ca/Al-D and high resolution P 2p XPS spectra (E) of IL-D, Ca/Al-D and C-Ca/Al-D. Adapted from [102].

Typical hexagonal morphology of all prepared Ca^{2+}/Al^{3+} LDH was shown in the SEM microphotographs (Fig. 9. A-D), which indicate that neither calcination nor organic modification with IL-D affected sizes (2-5 μm) and shapes of all LDH.

Thus, TGA of freshly dried Ca^{2+}/Al^{3+} LDH enabled to determine the exact content of water (10.15 wt.%, 10.89 wt.%, 0.57 wt.%, and 1.85 wt.% in Ca/Al, Ca/Al-D, C-Ca/Al, and C-Ca/Al-D, respectively), which may affect the course of εCL ROP. Moreover, for studying of the potential catalytic effect of IL-D, the exact concentrations of organic species in IL-modified LDH must be known. The IL-D amount was successfully determined by the combination of TGA (weight content of water), elemental analysis (carbon, nitrogen weight content) and XRF (calcium, aluminum weight content): 14.8 wt.% and 18.3 wt.% in Ca/Al-D and C-Ca/Al-D, respectively. Worth mentioning is that in case of Ca/Al-D, 14.8 wt.% referred to decanoate anions only, whereas 18.3 wt.% of organic species in C-Ca/Al-D reflected the content of whole IL-D (both phosphonium cation and decanoate anion).

4.2.2. Microwave-assisted ring opening polymerization of ε-caprolactone in the presence of ionic liquid-layered double hydroxides: kinetics and thermodynamics

In order to determine the role of decanoate anions, surface OH groups, and heating method in the course of εCL ROP, five reactions listed in Table 1 were carried out at constant temperature (170 °C) for 6 h (without any additional initiator or catalyst). As first, the MW-assisted ROP of εCL was conducted in the presence of pristine Ca/Al LDH (reaction A), where water acted as the initiator of polymerization. Generally, the water-initiated ROP of lactones as an example of ROP initiated by donor of proton can be described with pseudo-first order kinetics, which is expressed by linear relation of eq. 1:

$$ln\frac{C_0}{C} = f(t) = kt + b, \text{ eq. 1.}$$

Table 1. Ring opening polymerization of ε-caprolactone conducted in the presence of various Ca^{2+}/Al^{3+} LDH at 170 °C for 6 h. Adapted from [102].

Reaction no.	LDH type (wt.%)[a]	Heating method	[εCL]/[H_2O]	[εCL]/[IL^-][b]	α_t[c] [%]
A	Ca/Al (0.5)	MW	300/1	-	10
B	Ca/Al-D (0.5)	CH	300/1	2000/1	76
C	Ca/Al-D (0.5)	MW	300/1	2000/1	99
D-I	C-Ca/Al-D (0.5)	MW	1800/1	6000/1	11
D-II	Ca/Al-D (0.17)	MW	900/1	6000/1	11

[a]Weight content of LDH with reference to εCL. [b]Monomer/decanoate anion molar ratio.
[c]Final conversion of the monomer after t=6 h.

where C_0/C is a ratio of initial and immediate concentration of monomer as the function of time t and k (line slope) is a rate constant.

Kinetic data for the reaction A (Fig. 10. A) fitted well to eq. 1 confirming pseudo-first order reaction, which led to 10% of monomer conversion.

When Ca/Al-D was applied (reactions B and C), the achieved monomer conversion (α_t) was significantly increased (76-99%) regardless heating method. Nevertheless, much higher conversion was obtained for polymerization under MW irradiation (reaction C). This was a first indication of ROP acceleration evocated by a combination of IL and MW irradiation. The reaction with Ca/Al-D carried out under CH (Fig. 10. B) fitted to the pseudo-first order kinetics similarly to the reaction A (without IL). Contrary to this, the non-linear relation between $\ln(C_0/C)$ and the reaction time was obtained for the MW-assisted ROP in the presence of IL-intercalated LDH (reaction C, Fig. 10. C), thus evidencing a different mechanism and kinetics of polymerization.

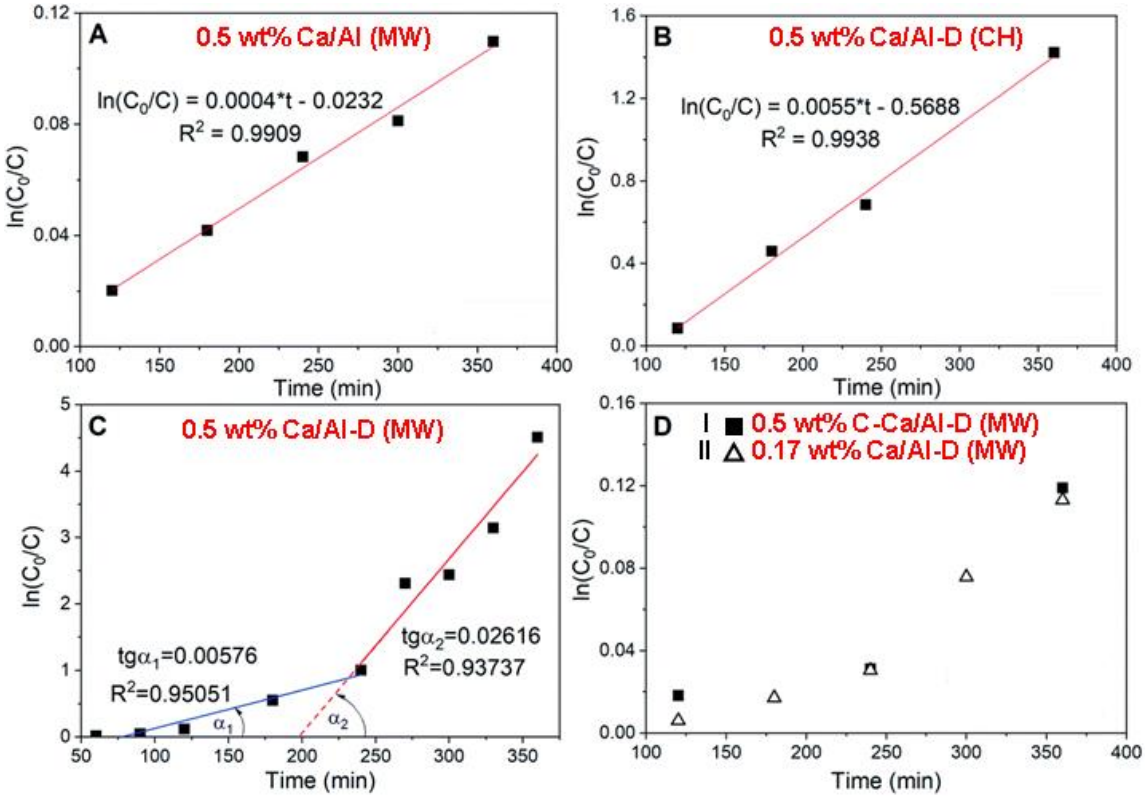

Fig. 10. Kinetic plots of εCL ROP conducted in the presence of: A – 0.5 wt.% Ca/Al under MW irradiation, B – 0.5 wt.% of Ca/Al-D under CH, C – 0.5 wt.% Ca/Al-D under MW irradiation, D-I – 0.5 wt.% of C-Ca/Al-D under MW irradiation and D-II – 0.17 wt.% of Ca/Al-D under MW irradiation [102].

A possible MW-assisted initiating effect of the OH groups located on the surface of hydrated Ca/Al-D was then investigated. The MW-assisted ROPs with i) calcinated (OH-free) C-Ca/Al-D (reaction D-I) and ii) hydrated Ca/Al-D (reaction D-II) were carried out, where the LDH contents were adjusted for the same concentration of decanoate anions in both reactions to have the same monomer/decanoate ratio (Table 1). The identical kinetic curves (Fig. 10. D-I and D-II) and the same monomer conversion (11%) of both reactions indicated that the surface OH groups were not involved in ROP, while the non-linear kinetics proved a synergy between MW

irradiation and IL previously observed for the reaction C. This synergistic effect was further studied using SAXS analysis (Fig. 11).

Initial polymerization mixture composed of 0.5 wt.% of Ca/Al-D dispersed in the monomer (pink curve in Fig. 11 denoted εCL+Ca/Al-D) showed the (002) reflection at ca. 3.0°. When MW irradiation was applied (series of SAXS profiles of the reaction mixture C after different reaction time on the top of Fig. 11), significant shift of the (002) reflection towards the lower θ was detected for the C reaction mixture after 60 min (Fig. 11, black curve) and 90 min (Fig. 11, red curve) indicating extension of basal spacing. At this reaction step, monomer molecules easily accessed between Ca/Al-D galleries, but the decanoate anions still remained screened by the calcium cations restricting their mobility. When the reaction time reached 120 min, the (002) reflection disappeared (Fig. 11, light green), which was assigned to the complete Ca/Al-D exfoliation resulting in release of the decanoate anions. Therefore, the degree of Ca/Al-D delamination was found to be a key factor affecting the rate of εCL ROP. The first ROP step was much slower since the catalytic species (decanoate anions) were immobilized between LDH galleries and thus much less accessible for the monomer molecules. In the second ROP step after LDH exfoliation (ca. 2 h), the decanoate anions became easily accessible for εCL molecules, which accelerated polymerization and resulted in rapid monomer consumption. After 3 and 4 h of the reaction, the formation of crystalline domains was observed (Fig. 11. dark and light blue SAXS profiles at 0.6° and 1.5°) indicating the presence of long PCL chains capable to crystallize.

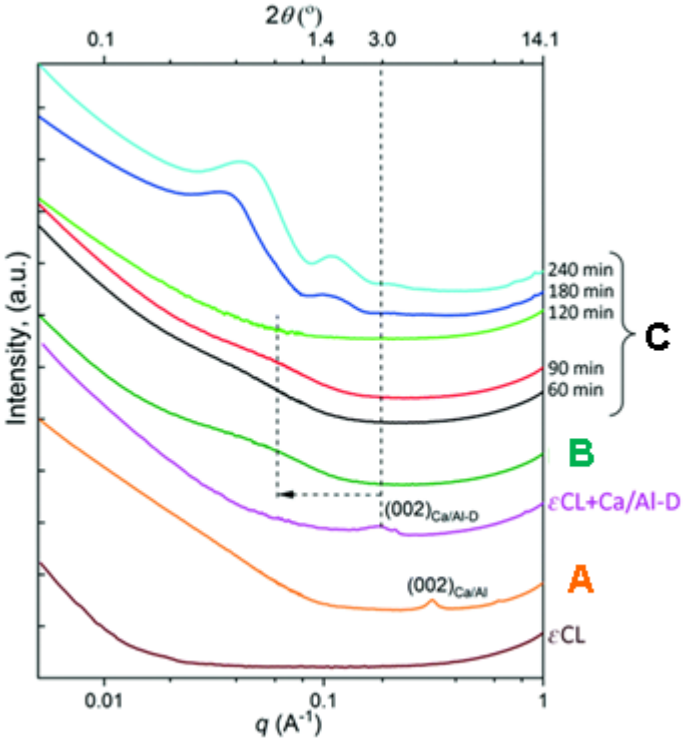

Fig. 11. SAXS profiles of pure monomer (εCL), dispersion of Ca/Al-D in εCL after sonication (εCL+Ca/Al-D) and reaction mixture of reaction A (0.5 wt.% Ca/Al, MW) after 2 h, reaction B (0.5 wt.% Ca/Al-D, CH) after 2h and reaction C (0.5 wt.% Ca/Al-D, MW) after selected reaction periods (60/90/120/180/240 min). Adapted from [102].

The SAXS analysis of the C reaction mixture revealed complete Ca/Al-D exfoliation after 2 h. After the same time, delamination of the non-modified Ca/Al under MW heating (orange SAXS profile in Fig. 11) and Ca/Al-D under CH (dark green SAXS profile in Fig. 11) was not complete. Only intercalated LDH structures were formed as it was indicated from the shift of the (002) reflections in case of both reactions (from 10.3° to ca. 4° and from 3.0° to ca. 0.7° in case of reaction A with Ca/Al and reaction B with Ca/Al-D, respectively). These observations correspond well with the pseudo-first order kinetics of reactions A and B (linear kinetic plots, Fig. 10) and reflect the course of εCL ROP similar to that in the presence of Ca/Al-D at the beginning, i.e. before Ca/Al-D exfoliation. Altogether, the synergy between the intercalated decanoate anions and the MW heating was confirmed: even though Ca/Al-D was applied in reaction B, its exfoliation under CH did not occur.

These findings indicate that εCL ROP conducted under MW irradiation in the presence of Ca/Al-D proceeds in two stages; the non-catalyzed (before LDH exfoliation) and the catalyzed with the decanoate anions, both showing a linear relation between $\ln(C_0/C)$ and t. The reaction rate constants for A, B and C were calculated from their kinetic plots: 0.0004 min^{-1} (A), 0.0055 min^{-1} (B), 0.0058 min^{-1} (the first stage of reaction C), and 0.0262 min^{-1} (the second stage of reaction C). In case of Ca/Al-D (reactions B and C), the reaction rate constants for ROP under CH (reaction B) and for the first stage of MW-assisted ROP (reaction C) were similar, which corresponded to the non-catalyzed step being the result of non-exfoliated Ca/Al-D structure. After complete exfoliation under MW irradiation (reaction C, the second stage), release of the decanoate anions accelerated the reaction (4.6-fold increase), which proved their catalytic effect on the water-initiated ROP of εCL.

Further kinetic analyses (Table 2) were performed for the series of εCL ROP at different Ca/Al-D weight contents (0.5%, 1.0% or 5.0%) and temperatures (130 °C, 150 °C, 170 °C or 190 °C). The reaction rate constants k_2 corresponding to the second ROP stage (after Ca/Al-D exfoliation and release of catalytic decanoate anions) at fixed LDH concentration insignificantly varied with temperature, which resulted in relatively low values of activation energies (E_a) for each LDH content. In comparison with the MW-assisted ROP of εCL conducted in the presence of super Brønsted acids at the same molar ratio of monomer/catalyst [26], the activation energy of εCL ROP catalyzed by decanoate-intercalated LDH (Ca/Al-D) was ca. 3 times lower indicating a strong catalytic effect of the decanoate anions.

ROP of εCL was further studied in terms of activation thermodynamics according to the transition state theory (so-called theory of activated complex) for bimolecular reactions [102]. According to this theory, complexes in the activated state can be characterized by the temperature-dependent Gibbs free energy $\Delta G_a^{\ddagger}$ according to Eyring-Polanyi equation (eq. 2: k_b – Boltzmann constant, h – Planck constant):

$$k = \frac{k_b T}{h} e^{\left(-\frac{\Delta G_a^{\ddagger}}{RT}\right)}, \text{ eq. 2.}$$

Table 2. Rate constant (k_2), activation energy (E_a), pre-exponential factor A, enthalpy ($\Delta H_a^{\ddagger}$) and entropy ($\Delta S_a^{\ddagger}$) of activation for MW-assisted εCL ROP conducted in the presence of Ca/Al-D at various temperatures and different LDH contents. Adapted from [102].

Ca/Al-D content (wt.%)	k_2 (s^{-1})				Arrhenius plot		Eyring–Polanyi plot	
	130 °C	150 °C	170 °C	190 °C	E_a (kJ mol^{-1})	A (s^{-1})	$\Delta H_a^{\ddagger}$ (kJ·mol^{-1})	$\Delta S_a^{\ddagger}$ (kJ·mol^{-1}·K^{-1})
0.5	—	$3.1 \cdot 10^{-4}$	$4.4 \cdot 10^{-4}$	$6.6 \cdot 10^{-4}$	30.7	1.89	27.1	−171.9
1.0	$6.5 \cdot 10^{-4}$	$8.1 \cdot 10^{-4}$	$8.8 \cdot 10^{-4}$	—	11.3	0.02	7.8	−92.5
5.0	$4.5 \cdot 10^{-3}$	$5.4 \cdot 10^{-3}$	$5.8 \cdot 10^{-3}$	—	9.3	0.07	5.8	−12.7

On the basis of eq. 2 and definition of Gibbs free energy, the values of enthalpy ($\Delta H_a^{\ddagger}$) and entropy ($\Delta S_a^{\ddagger}$) of εCL ROP activation were calculated (Table 2). Both thermodynamic parameters, enthalpy and entropy of activation, are related to the activation energy and the pre-exponential factor A, respectively. Since the pre-exponential factor represents entropic contribution, the largest A value (1.89 s^{-1}, from Arrhenius plot) for ROP conducted with 0.5 wt.% of Ca/Al-D corresponded well with the lowest entropy value (-171.9 kJ·mol^{-1}·K^{-1}) indicating that entropic change for the reaction at this Ca/Al-D content was the most preferable. On the other hand, enthalpic contribution at 0.5 wt.% of Ca/Al-D, represented by E_a, and $\Delta H_a^{\ddagger}$, were the highest, which resulted in the smallest k_2 values. At the higher LDH content (1.0/5.0 wt.%), differences between E_a and $\Delta H_a^{\ddagger}$ as well as A and $\Delta S_a^{\ddagger}$ were negligible. This is an indication, that the number of active species initiating εCL ROP was sufficient in the reaction mixture containing 1.0 wt.% of Ca/Al-D. Further increase of LDH content did not affect the reaction rate.

The negative values of activation entropy suggest a formation of active complex according to the associative mechanism, which occurs between two molecules (species) present in the polymerization system. It is in a good agreement with the assumed bimolecular activation of polymerization in terms of the transition state theory.

4.2.3. Mechanism of ε-caprolactone ring opening polymerization initiated/catalyzed by ionic liquid-functionalized layered double hydroxides

Generally, in case of all εCL ROP initiated/catalyzed by Ca/Al-D (regardless reaction temperature and LDH content), the conversion-time plots (Fig. 12. C) reveal the S-shaped α_t=f(t) curves which suggest slow initiation period being a limiting step of ROP. This phenomenon can be explained by i) a slow surface water desorption, ii) a limited monomer intercalation between Ca/Al-D layers in the beginning of the *in-situ* polymerization or iii) a time-dependent formation of active species (OH^- anions obtained from water self-dissociation). Based on these results and considerations, the non-catalyzed (Fig. 12. A) and the IL-catalyzed (Fig. 12. B) initiation of εCL

ROP by water was proposed. In both cases, the initiation proceeds via attack of hydroxyl anions (formed from water self-dissociation) on the carbonyl carbon atom of εCL resulting in opening of the monomer ring and formation of oxyanion active center able to attack a next monomer molecule. The non-catalyzed initiation (Fig. 12. A) corresponds to the first stage of ROP, when Ca/Al-D is not exfoliated. However, the intercalated water molecules can undergo self-dissociation forming H_3O^+ cations. They further react with the decanoate anions (Fig. 12. B) inducing re-creation of a more stable decanoic acid (small dissociation constant K_d, thus the equilibrium is shifted towards a neutral form). The consumption of H_3O^+ cations shifts the equilibrium of water self-dissociation towards the formation of ions, which leads to larger concentration of OH^- placed in the LDH galleries. These OH^- can further initiate ROP when the complete Ca/Al-D exfoliation is reached. Therefore, the catalytic effect of intercalated IL anions is connected with a direct formation of active species.

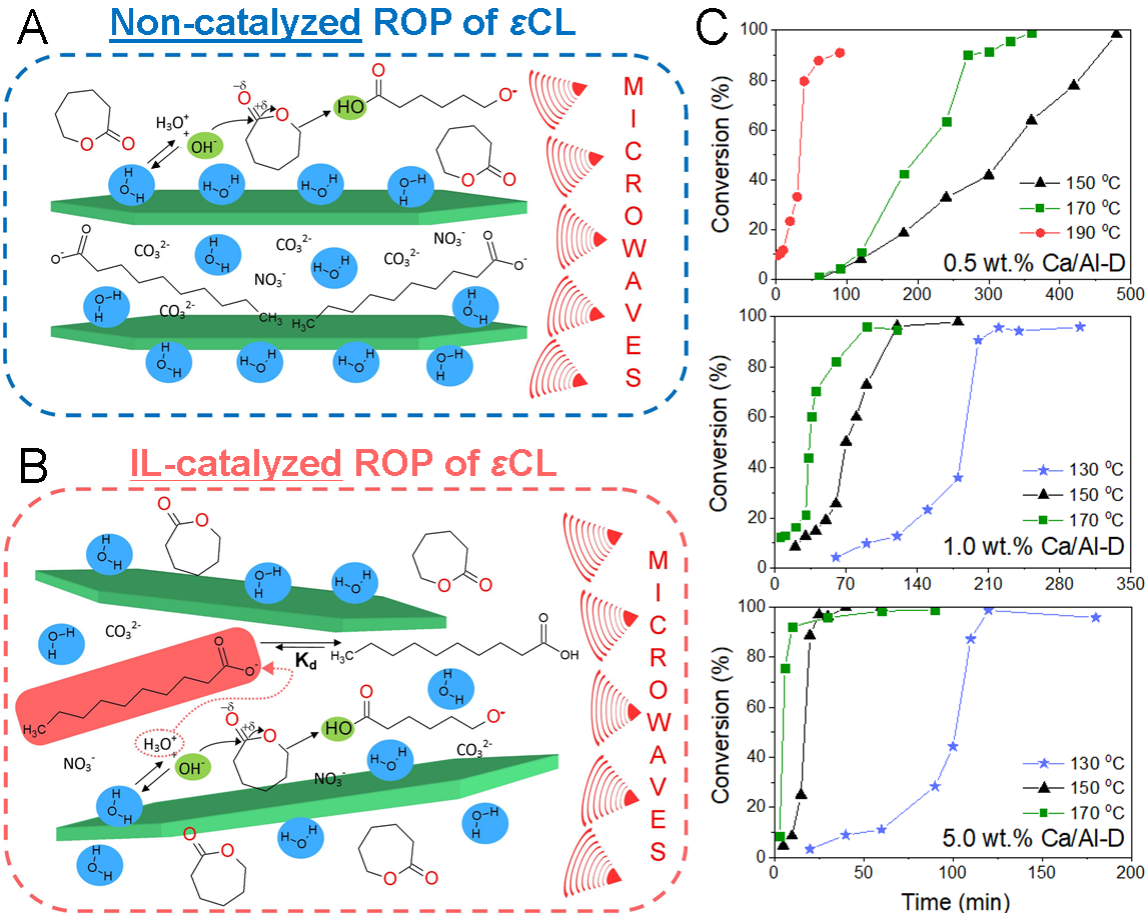

Fig. 12. Graphical presentation of non-catalyzed (A) and IL-catalyzed (B) εCL ROP in the presence of IL-modified LDH. Conversion-time plots (C) of εCL ROP with different Ca/Al-D content and at various reaction temperatures. Adapted from [102].

According to the revealed anionic mechanism of MW-assisted εCL ROP in the presence of IL-intercalated LDH, the propagation step proceeds up to total monomer consumption as confirmed by the vanishing of monomer signal on the GPC curve after 6 h (Fig. 13. B).

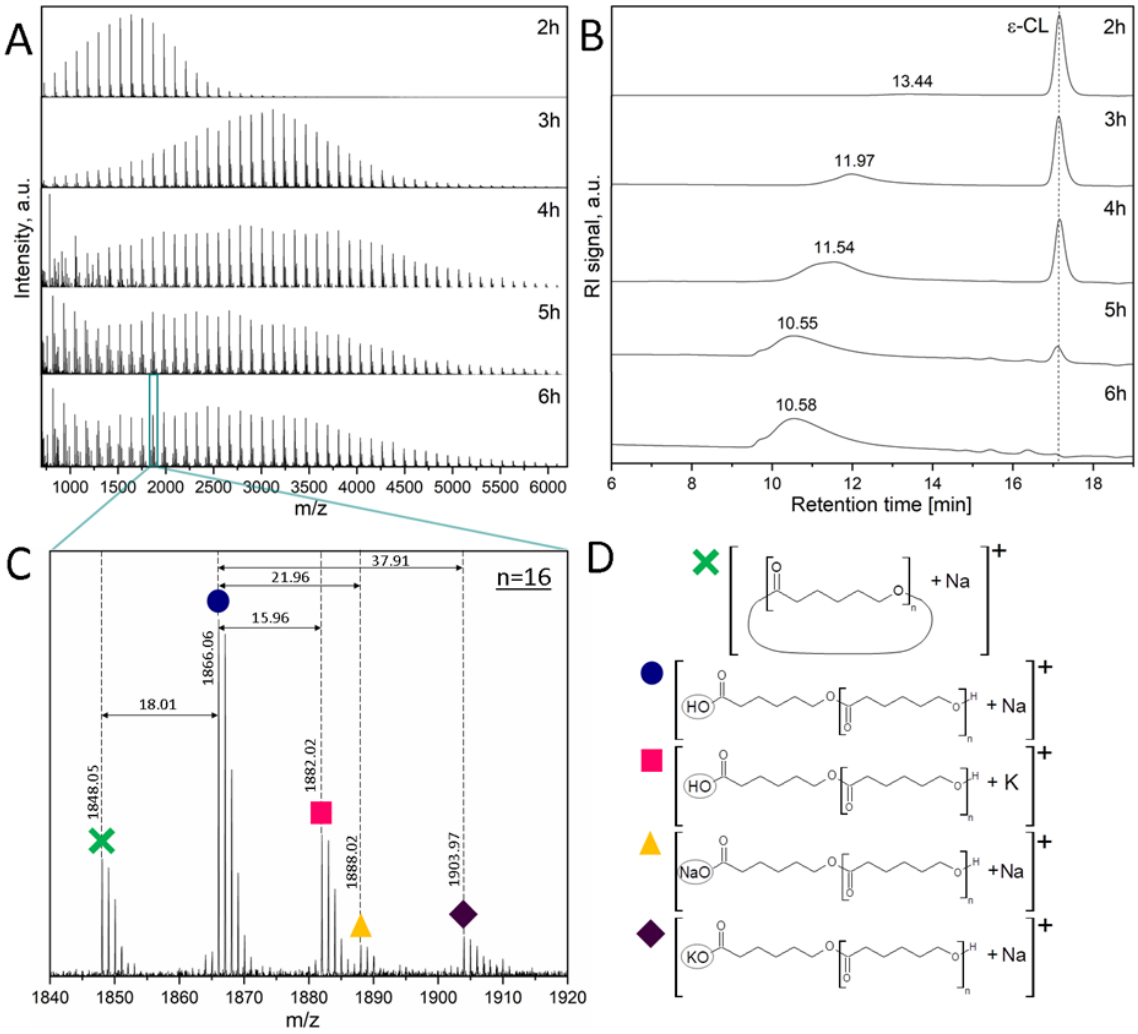

Fig. 13. MALDI-TOF mass spectra (A and C) with corresponding polymer structures (D) and GPC curves (B) during the MW-assisted ROP of εCL after 2 h, 3 h, 4 h, 5 h and 6 h at 170 °C in the presence of 0.5 wt.% LDH modified with decanoate anions (Ca/Al-D, reaction C). Adapted from [102].

The polymerization mixtures (after 2-6 h) were analyzed using MALDI-TOF mass spectrometry (Fig. 13. A and C). In the beginning of εCL ROP at low monomer conversions (Fig. 13. A. 2-3 h curves corresponding to α_t ca. 10-40 %), the propagation led to formation of linear PCL chains, while after 4 h the side reactions (back-biting) started to proceed, which resulted in a water release and formation of PCL macrocycles (the higher polymer dispersity observed by GPC and MALDI-TOF mass spectrometry, Fig. 13). Analysis of the final reaction products determined from the MALDI-TOF mass spectrum after 6 h revealed both the linear and the cyclic PCL structures (Fig. 13. D).

4.3. Properties of nanocomposites based on polycaprolactone and ionic liquid-layered double hydroxides: microwave-assisted *in-situ* polymerization vs. melt-blending

Appendix 3: *Effects of Immobilized Ionic Liquid on Properties of Biodegradable Polycaprolactone/LDH Nanocomposites Prepared by In Situ Polymerization and Melt-Blending Techniques*

The previous subsection 4.2 describes the effect of IL-functionalized LDH on the progress of MW-assisted εCL ROP. Beside the catalytic effect of IL-modified LDH, the immobilized IL and the MW irradiation synergistically promote LDH exfoliation. Therefore, the MW-assisted ROP can be considered as a promising environmental-friendly route for fabrication of the polymer nanocomposites. In this subsection, the influence of IL-modified LDH on structure and properties of PCL nanocomposites prepared by the MW-assisted *in-situ* εCL ROP is studied.

The above-described initiating effect of the intercalated water together with a relatively high water content (10.89 wt.%) in the Ca/Al-D causes that only a low molecular weight PCL ($\bar{M}_n$ ca. 20 000 g·mol^{-1}) with inferior mechanical properties can be produced by the *in-situ* εCL ROP. Therefore, the calcinated LDH containing 0.57 wt.% (C-Ca/Al) and 1.89 wt.% (C-Ca/Al-D) of water were selected for fabrication of PCL/LDH nanocomposites (ROP-series) via the MW-assisted *in-situ* εCL ROP. Conventional tin-based catalyst (tin(II) 2-ethylhexanoate) was added to accelerate ROP and to lower PCL dispersity. The corresponding PCL-LDH nanocomposites were also prepared by standard MB technique (MB-series as "reference samples" for comparison). The LDH content (1 wt.%) was selected on the basis of preliminary experiments as the maximum content of Ca-based LDH, at which the molecular weight of the *in-situ* synthesized PCL was high enough ($\bar{M}_n$ > 60 000 g·mol^{-1}, Table 3) for processing by compression molding (all samples were prepared as thin films, ~0.2 mm, for further testing and analyses).

Firstly, the influence of LDH and immobilized IL on the mechanical properties of the prepared nanocomposites was investigated (Table 3) on the MB-series of nanocomposite films, since they exhibited the similar values of molecular weight (Table 3), which was only slightly affected by thermal processing (compression molding). In case of film containing C-Ca/Al (MB-PCL+C-Ca/Al), the LDH addition decreased E, σ_{max}, and ε_{max}, which corresponded to the visible C-Ca/Al agglomerates and their low compatibility with polymer matrix. On the contrary, the σ_{max} and ε_{max} values of the film containing IL-functionalized LDH (MB-PCL+C-Ca/Al-D) were comparable to the neat PCL, which indicated better dispersibility of C-Ca/Al-D in PCL matrix compared to the non-modified C-Ca/Al, but still minor polymer-filler interactions. The slightly increased E (+5%) indicated the improved stiffness of this film.

In case of ROP-series, the slightly variable molecular weight of PCL matrix should be considered when comparing mechanical properties of these films. Although the addition of both C-Ca/Al and C-Ca/Al-D decreased the PCL M_n values (about ca. 20% and 40%, respectively; the larger M_n decrease in case of C-Ca/Al-D was related to the higher content of water in this LDH), the stiffness of both films (ROP-PCL+C-Ca/Al and ROP-PCL+C-Ca/Al-D) was significantly improved (+21% and +24%, respectively). This is a clear evidence of enhanced LDH dispersibility in the *is-situ* prepared nanocomposites compared to the MB nanocomposite films. The increased ε_{max} (+8.5%) of the nanocomposite containing IL-functionalized LDH (ROP-

PCL+C-Ca/Al-D) together with its significantly lower M_n value compared to the neat ROP-PCL indicated that IL-D acted as highly efficient interfacial agent inducing polymer-filler interactions.

Table 3. Mechanical properties, molecular weight ($\bar{M}_n$), dispersity ($Đ$) of neat PCL and PCL-LDH nanocomposites. Adapted from [103].

Sample	$\bar{M}_n \cdot 10^3$ [g·mol^{-1}]	$Đ$	Young modulus, E [MPa]	Tensile strength, σ_{max} [MPa]	Elongation at break, ε_{max} [%]
MB-PCL	126	1.2	443±9	33±3	424±22
MB-PCL+C-Ca/Al	117	1.3	434±8	29±5	382±59
MB-PCL+C-Ca/Al-D	120	1.3	465±10	32±2	419±19
ROP-PCL	99	1.4	463±13	28±1	390±13
ROP-PCL+C-Ca/Al	79	1.4	560±7	18±13	353±77
ROP-PCL+C-Ca/Al-D	61	1.6	572±26	25±2	423±23

Since PCL is a semicrystalline polymer, PCL crystallization may be induced by the addition of NPs acting as nucleating agents [54]. This phenomenon was investigated on the basis of Scherrer analysis of XRD nanocomposite film patterns [103]. According to Scherrer equation (eq. 3)

$$D_{(hkl)}=K\lambda\cdot(\beta cos\theta)^{-1}, \text{ eq. 3,}$$

where $D_{(hkl)}$ represents sizes of PCL crystalline domain sizes, K (0.9) – shape factor, and β – full width at half maximum of selected *hkl* reflection peak, the introduction of both C-Ca/Al and C-Ca/Al-D enhanced PCL crystallization regardless preparation method (Table 4, PCL crystalline domains in all nanocomposites were at least 2 times larger in comparison to the neat PCL). Nevertheless, the largest (2.8-fold) increase of PCL crystallites was observed for the ROP-synthesized nanocomposite film containing IL-functionalized LDH (ROP-PCL+C-Ca/Al-D). This indicated much better dispersibility of C-Ca/Al-D in the PCL matrix than that of C-Ca/Al.

Further evidence of the IL-functionalized LDH nucleating effect was observed from the crystallinity degree (X_c) differences for the series of MB nanocomposite films (Table 4). Negligible effect of the worse-dispersed C-Ca/Al on the PCL crystallization behavior (the similar X_c for neat MB-PCL and MB-PCL+C-Ca/Al) corresponded to the insignificant change of mechanical properties of the MB-PCL+C-Ca/Al film. On the contrary, the IL-functionalized LDH in MB-PCL+C-Ca/Al-D increased the PCL crystallinity (+9.2%). Although the absolute X_c values of ROP-PCL nanocomposite series are affected by the molecular weight of PCL matrix, it was clearly seen that C-Ca/Al-D induced the PCL crystallization more efficiently than C-Ca/Al (X_c was 37.2% and 42.9% for ROP-PCL+C-Ca/Al and ROP-PCL+C-Ca/Al-D, respectively). The XRD and DSC results confirmed the nucleating effect of both LDH; however, the better-dispersed IL-functionalized LDH (C-Ca/Al-D) was found to be more efficient for the PCL nucleation.

Surprisingly, the LDH addition did not significantly affect thermal properties of PCL-LDH nanocomposites. The alfa (glass) transition temperatures (T_α) remained similar to the neat PCL and all nanocomposite films were thermally stable up to ca. 300 ºC ($T_{d5\%}$ - temperature at the 5 % weight loss of the sample).

Table 4. Sizes of PCL crystalline domains $D_{(110)}$, thermal behavior and water contact angle of neat PCL and PCL-LDH nanocomposites. Adapted from [103].

Sample	$D_{(110)}$ [Å]	T_α [ºC]	T_m [ºC]	ΔH_m [J/g]	X_c [%]	$T_{d5\%}$ [ºC]	θ_{H2O} [º]
MB-PCL	73	-54.1	55.9	54.5	42.3	354.0	90±3
MB-PCL+C-Ca/Al	161	-54.4	53.6	59.6	42.8	307.1	81±4
MB-PCL+C-Ca/Al-D	179	-55.6	55.9	64.3	46.2	318.1	82±3
ROP-PCL	86	-57.5	53.6	65.1	46.8	304.3	81±1
ROP-PCL+C-Ca/Al	188	-56.8	55.4	51.2	37.2	308.0	75±3
ROP-PCL+C-Ca/Al-D	245	-55.4	56.9	59.0	42.9	318.7	79±2

T_α – main (glass) transition temperature (DMTA); T_m – melting temperature (DSC), ΔH_m – melting enthalpy, X_c – crystallinity; $T_{d5\%}$ – temperature of 5 % sample weight loss (TGA); θ_{H2O} – contact angle

The effect of rather hydrophilic LDH on the wettability of PCL-LDH nanocomposite films was further investigated using the measurement of water contact angle (θ_{H2O} in Table 4). For the MB-PCL series, the addition of both C-Ca/Al and C-Ca/Al-D decreased θ_{H2O} to the similar value (ca. 82º) indicating a more hydrophilic nature of the MB-PCL nanocomposites (regardless LDH type) than the neat MB-PCL (θ_{H2O}=90º). The nanocomposites prepared by ROP in the presence of C-Ca/Al (ROP-PCL+C-Ca/Al) exhibited the lower θ_{H2O} than that of the neat PCL (ROP-PCL) - similarly to the corresponding MB-PCL film (MB-PCL+C-Ca/Al). Contrary to this, the use of C-Ca/Al-D for *in-situ* ROP led to the nanocomposite (ROP-PCL+C-Ca/Al-D) with comparable hydrophilicity as that of the neat ROP-PCL. This can be indirect evidence of a more homogeneous dispersion of C-Ca/Al-D in the PCL matrix due to the presence of surface-bonded IL acting as a compatibilizer.

The permeation measurements of oxygen, carbon dioxide and water vapor through the PCL-LDH films were performed to evaluate barrier properties (Table 5). Regardless type of LDH and preparation method, the permeabilities (P) of penetrant molecules increased in the order: oxygen, carbon dioxide and water vapor, which corresponds to the growing polarity of these compounds. Generally, the higher P values for each penetrant were observed for the MB-PCL films. In case of ROP-PCL films, the introduction of non-modified LDH (C-Ca/Al) did not affect barrier properties of the prepared film (ROP-PCL+C-Ca/Al), whereas the addition of C-Ca/Al-D suppressed the permeation of all tested penetrants (about 17% in case of O_2 and CO_2 and 9% in case of water vapor) through ROP-PCL+C-Ca/Al-D. The decreased relative water vapor permeability of ROP-PCL+C-Ca/Al-D (WVP=0.91, Table 5) compared to the neat PCL indicates

the potential use of IL-LDH as a functional nanofiller for the PCL matrix improving its barrier properties. Considering its potential use for biodegradable packaging materials, MW-preparation of the PCL-LDH nanocomposites with a sufficiently high PCL molecular weight and a higher LDH loadings still remains a challenging issue due to a relatively high affinity of Ca-based LDH to water.

Table 5. Permeability coefficients *P* of PCL-LDH nanocomposite films for oxygen, carbon dioxide and water vapor, and relative water vapor permeability (WVP) for MB-PCL and ROP-PCL series. Relative WVP was calculated as ratio of *P* (H_2O) of the PCL-LDH nanocomposite and *P* (H_2O) of the neat PCL. Adapted from [103].

Sample	*P* (O_2) [Barrer]	*P* (CO_2) [Barrer]	*P* (H_2O) [Barrer]	Relative *WVP*
MB-PCL	1.18	13.1	939	-
MB-PCL+C-Ca/Al	1.22	13.9	1171	1.25
MB-PCL+C-Ca/Al-D	1.12	12.0	1058	1.13
ROP-PCL	0.96	10.1	826	-
ROP-PCL+C-Ca/Al	0.93	10.0	847	1.03
ROP-PCL+C-Ca/Al-D	0.80	8.4	755	0.91

Barrer = $1 \cdot 10^{-10}$ cm^3 (STP)$cm \cdot cm^{-2} \cdot s^{-1}$ $cmHg^{-1}$ = $3.3539 \cdot 10^{-16}$ $mol \cdot s^{-1} \cdot m^{-1} \cdot Pa^{-1}$

4.4. Microwave-assisted *in-situ* preparation of polycaprolactone-layered double hydroxide nanocomposites for packaging materials

Appendix 4: *Sustainable microwave synthesis of biodegradable active packaging films based on polycaprolactone and layered ZnO nanoparticles*

4.4.1. Layered double hydroxides as functional active nanofiller

Zn^{2+}/Al^{3+} LDH were selected for further MW-assisted preparation of PCL-LDH nanocomposites as an alternative to Ca-based LDH due to significantly lower Zn^{2+} affinity to water. The TGA results [104] showed that the Zn-based LDH contained 2.7-fold less water (0.7 wt.%) than Ca-based LDH, which enabled the higher Zn-based LDH loadings (>1 wt.%) for the *in-situ* εCL ROP.

Analogically to Ca-based LDH, Zn-based LDH (denoted ZnONPs) were functionalized with IL-D via surface modification leading to IL-ZnONPs with surface-bonded IL as confirmed by FTIR (Fig. 14. A, red curve: C-H stretching vibrations at 2928-2858 cm^{-1} and carboxylate vibrations at 1574 cm^{-1}). The crystallographic patterns of both non-modified ZnONPs (Fig. 14. B, blue curve) and IL-functionalized ZnONPs (Fig. 14. B, red curve) reveal a crystalline structure corresponding mainly to the zinc oxide in the shape of 2D hexagonal sheets of ca. 5 μm size and nanometric thickness (Fig. 14. C). Thus, the morphology of prepared ZnONPs was analogical to the previously used Ca-based LDH, whereas the content of immobilized IL-D in IL-ZnONPs (estimated on the basis of TGA results) was twice lower than in C-Ca/Al-D [104].

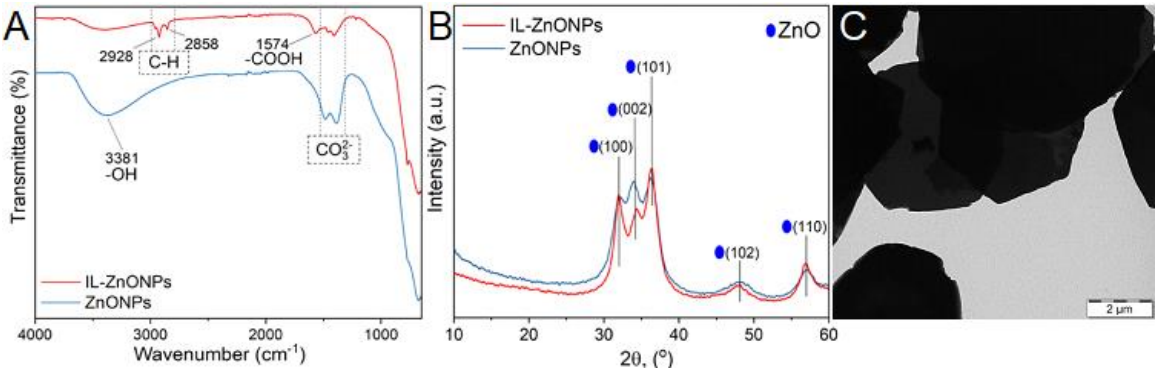

Fig. 14. FTIR spectra (A) and XRD patterns (B) of ZnONPs (blue curve) and IL-ZnONPs (red curve). Morphology of ZnONPs on the TEM microphotograph (C). Adapted from [104].

The additional advantage of NPs based on ZnO is a possibility to prepare antimicrobial nanocomposites containing ZnONPs due to a well-known antibacterial effect of zinc oxide [105].

4.4.2. Application-related properties of *in-situ* prepared polycaprolactone-layered double hydroxide nanocomposites

The series of PCL nanocomposites containing both non-modified ZnONPs and IL-functionalized ZnONPs (IL-ZnONPs) at various NPs loadings (1-4 wt.%) were prepared via the MW-assisted *in-situ* εCL ROP and subsequently processed by the compression molding to receive thin (0.2 mm thick) films. Despite the higher loadings of ZnONPs (up to 2 wt.%) and IL-ZnONPs (up to 3 wt.%), the prepared PCL-ZnONPs nanocomposites were easily processable due to the lower molecular weight (Table 6, $\bar{M}_n$ = 30 000 – 50 000 g·mol^{-1}) in comparison to the PCL-LDH nanocomposites with Ca-based LDH ($\bar{M}_n$ was ca. 60 000 g·mol^{-1}). At the highest NPs loadings (3 wt.% of ZnONPs and 4 wt.% of IL-ZnONPs), the nanocomposites were too brittle for processing (due to too low $\bar{M}_n$, Table 6) and therefore they were characterized by DSC only.

Table 6. Crystalline domain sizes ($D_{(110)}$), degree of crystallinity (X_c), molecular weight ($\bar{M}_n$), dispersity ($Đ$) and mechanical properties of PCL-ZnONPs films. Adapted from [104].

Sample	$\bar{M}_n \cdot 10^3$ [g·mol^{-1}]	$Đ$	$D_{(110)}$ [Å]	X_c [%]	Young modulus, E [MPa]	Tensile strength, σ_{max} [MPa]	Elongation at break, ε_{max} [%]
1% ZnONPs	41.1	1.7	354	47.4	634±22	15±1	163±74
2% ZnONPs	29.8	1.8	344	48.0	773±41	15±1	3±0
3% ZnONPs	19.8	1.7	-	53.5	-	-	-
1% IL-ZnONPs	49.6	1.8	341	44.6	551±54	20±7	332±138
2% IL-ZnONPs	33.2	1.9	338	48.2	744±44	14±2	4±1
3% IL-ZnONPs	32.7	1.6	342	46.7	843±38	7±4	1±1
4% IL-ZnONPs	17.5	1.8	-	51.4	-	-	-

Generally, the PCL crystalline domains formed in all PCL-ZnONPs nanocomposites were much larger than those in the nanocomposites with Ca-based LDH (80-250 Å). However, the

content and type (the presence of surface-bonded IL-D) of NPs had indiscernible influence on the sizes of PCL crystallites in the PCL-ZnONPs nanocomposite films (Table 6). On the contrary, the degree of crystallinity increased with the increasing NPs loading and reached much higher values (ca. 47-54%) in comparison with the commercial PCL (X_c=42.3% for MB-PCL). Both ZnONPs and IL-ZnONPs thus exhibited the nucleating effect.

The tensile test of PCL-ZnONPs films (denoted 1/2% ZnONPs and 1/2/3% IL-ZnONPs) revealed the higher rigidity (E) of nanocomposite films with the increasing content of both NPs. Thus, the stiffness of PCL-ZnONPs films was improved by introduction of NPs despite their negative effect on the PCL molecular weight (Table 6). However, the significant drop of σ_{max} and ε_{max} with the increasing NPs loadings reflected the growing brittleness of nanocomposites containing 2 wt.% or 3 wt.% of NPs. The comparison of mechanical properties of the nanocomposites with 1 wt.% of NPs (1% ZnONPs and 1% IL-ZnONPs) showed that the surface-bonded IL-D significantly improved σ_{max} and ε_{max} about 36% and 104%, respectively. It demonstrated better compatibility and more homogenous distribution of IL-ZnONPs in the PCL matrix.

Subsequently, the barrier properties of the prepared nanocomposite films were investigated to determine whether the higher NPs content in PCL-ZnONPs caused the targeted reduction of gas/water vapor permeability (Fig. 15).

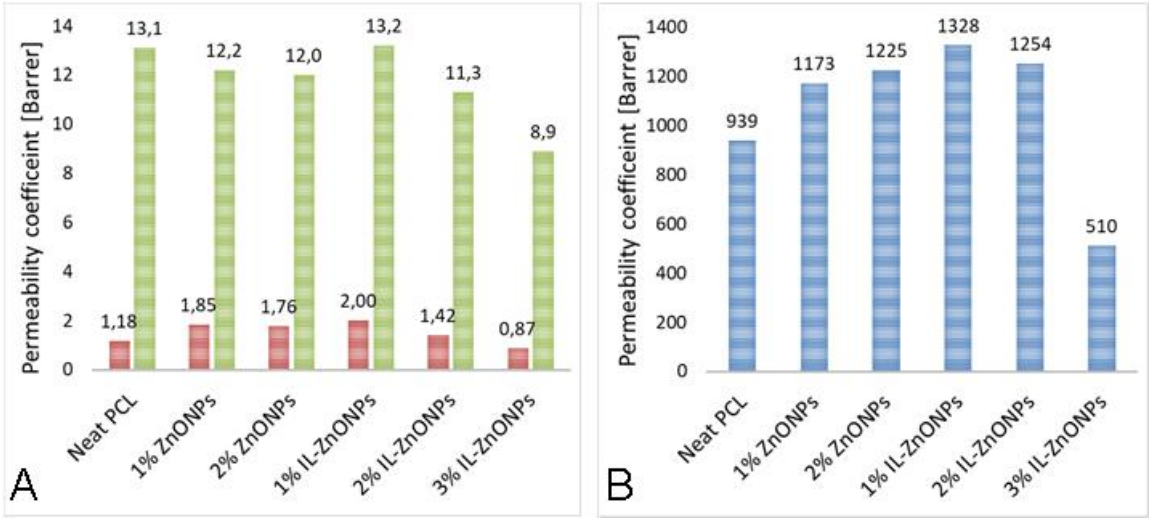

Fig. 15. Permeability coefficient P for O_2 (A, red), CO_2 (A, green) and water vapor (B). Adapted from [104].

The P coefficients of the PCL-ZnONPs films increased in the order of O_2<CO_2<<H_2O, similarly to the PCL-LDH nanocomposites containing Ca-based LDH (subsection 4.3). Oxygen and carbon dioxide transport through the PCL-ZnONPs films was merely slightly affected by the presence of both NPs. In contrast, the NPs effect on the water vapor permeability (WVP) was more significant: while the PCL-ZnONPs films with 1 wt.% or 2 wt.% of NPs exhibited comparable WVP to the commercial PCL, the 3% IL-ZnONPs nanocomposite film exhibited a

dramatical WVP drop, reaching the relative WVP of 0.54. At 3 wt.% loading of IL-ZnONPs the permeability values of all penetrants significantly decreased (26% for O_2, 32% for CO_2). Therefore, this sample was found to be the most promising for potential application as a biodegradable packaging material with the improved barrier properties.

The further application-related test was focused on the antimicrobial effect of PCL-ZnONPs nanocomposite films against the food-borne pathogenic bacterium *E. coli*. The test was evaluated as the suppression of *E. coli* biofilm development (expressed as PCL-ZnONPs surface coverage) after 4, 8, and 24 h (Fig. 16). The initial surface coverage (after 4 h) was the highest for the neat PCL (11.8±2.4%) and gradually decreased with the increasing ZnONPs or IL-ZnONPs addition. The smallest surface coverage (2.8±0.6%) was obtained for the 3% IL-ZnONPs nanocomposite film. The same trend was observed after 8 and 24 h. E.g. the bacterial growth on the nanocomposite film with 3 wt.% of IL-ZnONPs was significantly suppressed after 24 h (39.0±2.2%) compared to the *E. coli* growth on the neat PCL surface (67.1±6.%). These results demonstrated the antibacterial effect of the nanocomposite surfaces containing IL-ZnONPs, which was correlated to the increasing loading of IL-functionalized NPs. Since the bacterial growth is more preferential on hydrophilic surfaces, the suppressing *E. coli* adhesion on the films containing IL-ZnONPs was related to the surface-bonded IL-D, which decreased a material hydrophilicity.

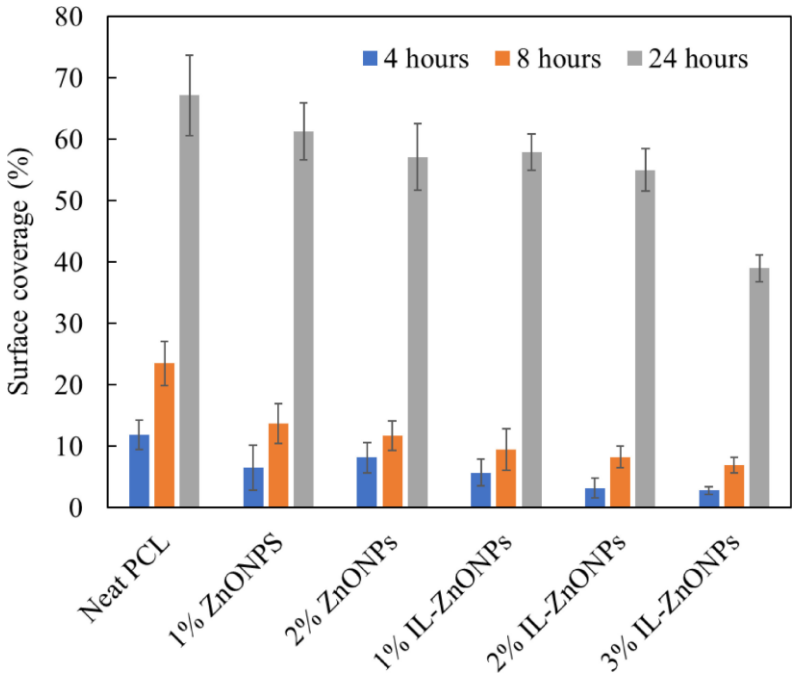

Fig. 16. Development of *E. coli* biofilm formation on PCL-ZnONPs films (after 4, 8 and 24 h cultivation time). Adapted from [104].

The effect of NPs addition on biodegradation of the prepared nanocomposites was also evaluated using the *in-vitro* 4-week test under the laboratory conditions (Fig. 17). This test is generally considered as a fast (screening) test prior to compost/soil biodegradation tests, which

are much more time-consuming (6 months). To simulate natural compost/soil conditions, a mixture of soil-isolated microorganisms, fungus *Fusarium solani* and bacterium *Pseudomonas sp.*, was selected. No visible degradation of the neat PCL and the 1% IL-ZnONPs films was observed after 4 weeks (Fig. 17. a, d). Contrary to this, a noticeable biodegradation of the nanocomposites containing ZnONPs (1 wt.% and 2 wt.% in Fig. 17. b and c, respectively) and 2 wt.% or 3 wt.% of IL-ZnONPs (Fig. 17. e and f) was observed after the same time.

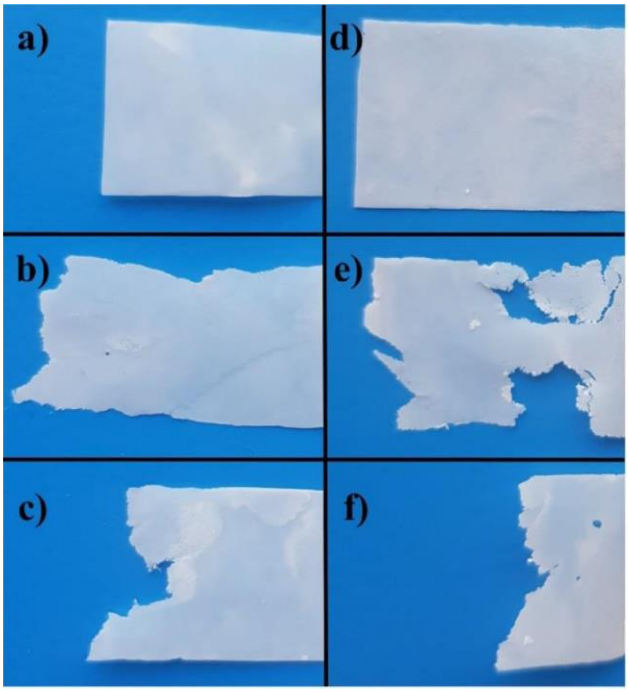

Fig. 17. PCL-ZnONPs films: a) neat PCL, b) 1% ZnONPs, c) 2% ZnONPs, d) 1% IL-ZnONPs, e) 2% IL-ZnONPs, and f) 3% IL-ZnONPs after 4 weeks biodegradation test with mixed microorganisms cultures (bacterium *Pseudomonas sp.* and fungus *Fusarium solani*). Adapted from [104].

Generally, a preferential degradation of semicrystalline PCL occurs in the amorphous phase due to the enhanced water sorption and the easier access of microorganisms to ester linkages. During the course of biodegradation, the PCL chains are cleaved resulting in the increase of overall sample crystallinity. For all tested PCL-ZnONPs films, the values of X_c (determined from DSC) increased about 2.7-4.8% after 4 weeks. The neat PCL film showed the highest X_c increase due to the lowest initial X_c of this film. The X_c values of the nanocomposite films containing the IL-functionalized NPs (IL-ZnONPs) increased after 4 weeks of biodegradation in relation to the NPs content: 3.0%, 2.7%, and 4.3% for 1 wt.%, 2 wt.%., and 3 wt.% of NPs, respectively. During the course of biodegradation, the PCL dispersity ($Đ$) is decreased due to preferential cleavage of short PCL chains. The decreasing $Đ$ values were observed for the PCL-ZnONPs film containing 2 wt.% of ZnONPs and the whole series of IL-ZnONPs films, while the $Đ$ values of the neat PCL and the 1% ZnONPs remained unaffected.

To sum up, the processable PCL nanocomposites with relatively high content of NPs were successfully prepared via the MW-assisted *in-situ* εCL ROP in the presence of IL-ZnONPs. The

nanocomposite film containing 3 wt.% of IL-ZnONPs showed significantly reduced gas/water vapor permeation, suppressed microbial growth of pathogenic *E.coli* and accelerated biodegradation in comparison to the neat PCL.

5. Conclusion

Experiments carried out in this thesis revealed that:

- direct co-precipitation synthesis of IL-functionalized Mg^{2+}/Al^{3+} LDH led to inhomogeneous, partially IL-intercalated LDH structure,
- IL-functionalization of Ca^{2+}/Al^{3+} LDH conducted via AE reaction led to homogenous fully IL-intercalated LDH structure without presence of surface-bonded IL,
- complete IL-LDH exfoliation was merely achieved under MW, which indicated synergistic effect of intercalated IL anion and MW irradiation,
- decanoate intercalated Ca^{2+}/Al^{3+} LDH acted as initiating/catalytic system for *in-situ* εCL ROP under MW: adsorbed/intercalated water initiated polymerization, IL anions showed catalytic effect,
- *in-situ* εCL ROP under MW proceeded according to pseudo-first order kinetics in two stages: non-catalyzed (before IL-LDH exfoliation) and IL-catalyzed (after complete IL-LDH exfoliation),
- *in-situ* synthesized PCL was composed of linear chains ended with –COOH and –OH groups as well as macrocycles,
- calcinated Ca-based LDH having lower water content than hydrated Ca^{2+}/Al^{3+} LDH were more suitable for *in-situ* εCL ROP, because they provided sufficiently high molecular weight of PCL,
- maximum loading of calcinated Ca-based LDH for MW-assisted *in-situ* preparation of PCL-LDH nanocomposites was 1 wt.%,
- IL improved IL-LDH dispersibility and induced polymer-filler interactions in case of *in-situ* prepared PCL-LDH nanocomposites,
- IL-LDH enhanced PCL nucleation,
- calcinated Zn-based LDH exhibited 3 times lower water content and can be applied for MW-assisted *in-situ* εCL ROP up to 3 wt.%,
- IL-ZnONPs significantly improved water vapor barrier properties, suppressed growth of *E. coli* and enhanced biodegradation of PCL nanocomposite containing 3 wt.% of nanofiller.

Relatively high content of water leading to lowering of PCL molecular weight and gaining the nanocomposites with insufficient mechanical properties is the main limitation of using LDH for the *in-situ* εCL ROP. However, this issue was overcome by synthesizing of IL-functionalized NPs based on antibacterial ZnO, which exhibited the lowest affinity to water and could be applied for the MW-assisted *in-situ* εCL ROP at higher loadings. Sustainable MW-assisted synthesis of biodegradable and antimicrobial PCL nanocomposites with improved barrier properties indicated a great application potential of PCL-ZnONPs for active bio-packaging.

This thesis also provided novel valuable findings about IL-functionalization of LDH depending on their chemical composition and proposed how to determine location (surface or interlayer space) and precise concentration of introduced organic species.

Experience and knowledge gained during this doctoral thesis enables to design task-specific functionalized NPs and apply them in MW-assisted polymer syntheses leading to nanocomposites with tunable application-related properties. As the future perspective, nanocomposites based on biodegradable polymer matrix and ZnO functionalized with naturally occurring antioxidants (e.g. polyphenols) providing another advantageous function to the *in-situ* MW-synthesized active materials will be the subject of interest. Moreover, novel type of NPs called layered double alkoxides, which are structurally similar to herein used LDH, may become interesting alternatives since these NPs can be synthesized as water-free.

Publications

Papers included in this thesis:

1. Beneš, H., Kredatusová, J., Peter, J., Livi, S., **Bujok, S.**, Pavlova, E., Hodan, J., Abbrent, S., Konefał, M., Ecorchard, P. (2019). Ionic liquids as delaminating agents of layered double hydroxide during in-situ synthesis of poly (butylene adipate-co-terephthalate) nanocomposites. *Nanomaterials*, 9(4), 618 (IF=4.324)
2. **Bujok, S.**, Konefał, M., Abbrent, S., Pavlova, E., Svoboda, J., Trhlíková, O., Walterová, Z., Beneš, H. (2020). Ionic liquid-functionalized LDH as catalytic-initiating nanoparticles for microwave-activated ring opening polymerization of ε-caprolactone. *Reaction Chemistry & Engineering*, 5(3), 506-518 (IF=3.441)
3. **Bujok, S.**, Hodan, J., Beneš, H. (2020). Effects of Immobilized Ionic Liquid on Properties of Biodegradable Polycaprolactone/LDH Nanocomposites Prepared by In Situ Polymerization and Melt-Blending Techniques. *Nanomaterials*, 10(5), 969 (IF=4.324)
4. **Bujok, S.**, Peter, J., Halecký, M., Ecorchard, P., Machálková, A., Santos Medeiros, G., Hodan, J., Pavlova, E., Beneš, H. (2021). Sustainable microwave synthesis of biodegradable active packaging films based on polycaprolactone and layered ZnO nanoparticles. *Polymer Degradation & Stability*, 190, 109625 (IF=4.032)

Other publications:

5. Mielczarek, K., Łabanowska, M., Kurdziel, M., Konefał, R., Beneš, H., **Bujok, S.**, Kowalski, G., Bednarz, S. (2020). High-Molecular-Weight Polyampholytes Synthesized via Daylight-Induced, Initiator-Free Radical Polymerization of Renewable Itaconic Acid. *Macromolecular rapid communications*, 41(4), 1900611 (IF=4.886)
6. Skleničková, K., Vlčková, V., Abbrent, S., **Bujok, S.**, Paruzel, A., Kanizsová, L., Trhlíková, O., Říhová Ambrožová, J., Halecký, M., Beneš, H. (2021). Open-Cell Aliphatic Polyurethane Foams with High Content of Polysaccharides: Structure, Degradation, and Ecotoxicity. *ACS Sustainable Chemistry & Engineering*, 9(17), 6023–6032 (IF=7.632)
7. **Bujok, S.**, Konefał, M., Konefał, R., Nevoralová, M., Bednarz, S., Mielczarek, K., Beneš, H. Insight into the aqueous Laponite® nanodispersions for self-assembled poly(itaconic acid) nanocomposite hydrogels: the effect of multivalent phosphate dispersants. *Journal of Colloid and Interface Science* (IF=7.489) – under review

Patent applications:

1. Beneš, H., **Bujok, S.**, Paruzel, A., Zajícová, V., Hnátková, T., Busscher G., F., Schmeets A. A., J. Biodegradable polyurethane foam, biodegradable polyurethane foam-based material for saccharide-cleaving enzyme production, method of synthesis and use thereof. International PCT Patent Application, PCT/CZ2021/050007 (submitted 2021).
2. Beneš, H., **Bujok, S.**, Paruzel, A., Zajícová, V., Hnátková, T., Busscher G., F., Schmeets A. A., J. Biodegradovatelná polyuretanová pěna, materiál na bázi biodegradabilní polyuretanové pěny pro produkci enzymů štěpících sacharidy, způsob jejich přípravy a jejich použití. PV 2020-32 (submitted 2020).

Conference contributions

Results of my work were presented on four conferences:

1. **Bujok, S.**, Beneš, H., Kredatusová, J., Konefał, M., Pavlova, E., Ecorchard, P. Functionalization of layered double hydroxide for in-situ ring opening polymerization (poster)
   9th Green Chemistry and Nanotechnologies in Polymeric Materials, Cracow, Poland, 10-12.10.2018
2. **Bujok, S.**, Beneš, H., Konefał, M., Pavlova, E., Ecorchard, P.
   Roles of LDH-ionic liquids in PCL nanocomposites preparation: in-situ polymerization vs. melt-intercalation (poster)
   International Symposium: 6th Frontiers in Polymer Science, Budapest, Hungary, 5-8.5.2019
3. Beneš, H., **Bujok, S.**, Skleničková, K., Pražanová, K., Innemanová, P., Kanizsová, L., Halecký, M., Kočí, V.
   Polyurethane foams for environmental applications (presentation, co-author)
   10th Green Chemistry and Nanotechnologies in Polymeric Materials, Riga, Latvia, 9.-11.10.2019
4. **Bujok, S.**, Konefał, M., Nováková, S., Pavlova, E., Svoboda, J., Trhlíková, O., Walterová, Z., Hodan, J., Beneš, H.
   Roles of immobilized ionic liquid on synthesis and properties of biodegradable nanocomposites (presentation, co-author)
   1st ECNP Workshop on Progress in Nanostructured Polymers, Lodz, Poland, 14.12.2020

Appendices

Herein listed papers together with corresponding supplementary materials are attached in the form of appendices at the end of this thesis:

1. Beneš, H., Kredatusová, J., Peter, J., Livi, S., **Bujok, S.**, Pavlova, E., Hodan, J., Abbrent, S., Konefał, M., Ecorchard, P. (2019). Ionic liquids as delaminating agents of layered double hydroxide during in-situ synthesis of poly (butylene adipate-co-terephthalate) nanocomposites. *Nanomaterials*, 9(4), 618 (IF=4.324)
2. **Bujok, S.**, Konefał, M., Abbrent, S., Pavlova, E., Svoboda, J., Trhlíková, O., Walterová, Z., Beneš, H. (2020). Ionic liquid-functionalized LDH as catalytic-initiating nanoparticles for microwave-activated ring opening polymerization of ε-caprolactone. *Reaction Chemistry & Engineering*, 5(3), 506-518 (IF=3.441)
3. **Bujok, S.**, Hodan, J., Beneš, H. (2020). Effects of Immobilized Ionic Liquid on Properties of Biodegradable Polycaprolactone/LDH Nanocomposites Prepared by In Situ Polymerization and Melt-Blending Techniques. *Nanomaterials*, 10(5), 969 (IF=4.324)
4. **Bujok, S.**, Peter, J., Halecký, M., Ecorchard, P., Machálková, A., Santos Medeiros, G., Hodan, J., Pavlova, E., Beneš, H. (2021). Sustainable microwave synthesis of biodegradable active packaging films based on polycaprolactone and layered ZnO nanoparticles. *Polymer Degradation & Stability*, 190, 109625 (IF=4.032)

References

[1] Urbánek, T., Jäger, E., Jäger, A., Hrubý, M. (2019). Selectively biodegradable polyesters: Nature-inspired construction materials for future biomedical applications. *Polymers*, 11(6), 1061

[2] Kliem, S., Kreutzbruck, M., Bonten, C. (2020). Review on the biological degradation of polymers in various environments. *Materials*, 13(20), 4586

[3] Tian, H., Wu, F., Chen, P., Peng, X., Fang, H. (2020). Microwave-assisted *in situ* polymerization of polycaprolactone/boron nitride composites with enhanced thermal conductivity and mechanical properties. *Polymer International*, 69(7), 635–643

[4] Sosnik, A., Gotelli, G., Abraham, G. A. (2011). Microwave-assisted polymer synthesis (MAPS) as a tool in biomaterials science: How new and how powerful. *Progress in Polymer Science*, 36(8), 1050–1078

[5] Hayes, B. L. (2002). *Microwave synthesis: chemistry at the speed of light*, 1st ed. New York: CEM Publishing

[6] Bogdał, D., Prociak, A. (2008). *Microwave-enhanced polymer chemistry and technology*, 1st ed. Wiley-Blackwell

[7] Kempe, K., Becer, C. R., Schubert, U. S. (2011). Microwave-assisted polymerizations: Recent status and future perspectives. *Macromolecules*, 44(15), 5825–5842

[8] Zhou, Y.-N., Li, J.-J., Wu, Y.-Y., Luo, Z.-H. (2020). Role of External Field in Polymerization: Mechanism and Kinetics. *Chemical Reviews*, 120(5), 2950–3048

[9] Herrera-Kao, W. A., Aguilar-Vega, M. J., Cervantes-Uc, J. M. (2020). Microwave-assisted synthesis of the lipase-catalyzed ring-opening copolymerization of ε-caprolactone and ω-pentadecanolactone: Thermal and FTIR characterization. *e-Polymers*, 20(1), 651–658

[10] Sivalingam, G., Agarwal, N., Madras, G. (2004). Kinetics of Microwave-Assisted Polymerization of ε-Caprolactone." *Journal of Applied Polymer Science*, 91(3), 1450–1456

[11] Kojić, D., Erceg, T., Vukić, N., Teofilović, V., Ristić, I., Budinski-Simendić, J., Aleksić, V. (2017). The catalytic microwave synthesis of biodegradable polyester polyols based on castor oil and l-lactide. *IOP Conference Series: Materials Science and Engineering*, 163(1), 12048

[12] Dubey, S. P., Thakur, V. K., Krishnaswamy, S., Abhyankar, H. A., Marchante, V., Brighton, J. L. (2017). Progress in environmental-friendly polymer nanocomposite material from PLA: Synthesis, processing and applications. *Vacuum*, 146, 655–663

[13] Nguyen, H. L., Vu, T. T., Nguyen, D.-K., Trickett, C. K., Doan, T. L. H., Diercks, C. S., Nguyen, V. T., Cordova, K. E. (2018). A complex metal-organic framework catalyst for microwave-assisted radical polymerization. *Communications Chemistry*, 1(70), 1–7

[14] Xie, Z.-K., Guo, J.-K., Luo, Z.-H. (2018). Assessment of Microwave Effect on Polymerization Conducted under ARGET ATRP Conditions. *Macromolecular Reaction Engineering*, 12(1), 1700032

[15] Chen, F., Wang, J., Chen, H., Lu, R., Xie, X. (2018). Microwave-assisted RAFT polymerization of well-constructed magnetic surface molecularly imprinted polymers for specific recognition of benzimidazole residues. *Applied Surface Science*, 435, 247–255

[16] Fan, F., Cai, C., Gao, L., Li, J., Zhang, P., Li, G., Li, C., Yu, G. (2017). Microwave-assisted synthesis of glycopolymers by ring-opening metathesis polymerization (ROMP) in an emulsion system. *Polymer Chemistry*, 8(44), 6709–6719

[17] Temur Ergan B., Bayramoğlu, M. (2018). Poly(l-lactic acid) synthesis using continuous microwave irradiation–simultaneous cooling method. *Chemical Engineering Communications*, 205(12), 1665–1677

[18] von Seggern, N., Schindler, T., Naumann, S. (2020). Dual Catalytic Ring-Opening Polymerization of Ethylene Carbonate for the Preparation of Degradable PEG. *Biomacromolecules*, 21(7), 2661–2669

[19] Liao, L., Zhang, C., Gong, S. (2007). Microwave-assisted ring-opening polymerization of trimethylene carbonate in the presence of ionic liquid. *Journal of Polymer Science, Part A: Polymer Chemistry*, 45(24), 5857–5863

[20] Petit, C., Grassl, B., Mignard, E., Luef, K. P., Wiesbrock, F., Reynaud, S. (2017). Living cationic ring-opening polymerization of 2-ethyl-2-oxazoline following sustainable concepts: Microwave-assisted and droplet-based millifluidic processes in an ionic liquid medium. *Polymer Chemistry*, 8(38), 5910–5917

[21] Fang, X., Simone, C. D., Vaccaro, E., Huang, S. J., Scola, D. A. (2002). Ring-opening polymerization of ε-caprolactam and ε-caprolactone via microwave irradiation. *Journal of Polymer Science, Part A: Polymer Chemistry*, 40(14), 2264–2275

[22] Fimberger M., Wiesbrock, F. (2014). Microwave-Assisted Synthesis of Polyesters and Polyamides by Ring-Opening Polymerization. In: Hoogenboom, R., Schubert, U., Wiesbrock, F. *Microwave-assisted Polymer Synthesis. Advances in Polymer Science*, vol. 274, Eds. Springer, Cham

[23] Liao, L. Q., Liu, L. J., Zhang, C., He, F., Zhuo, R. X. (2003). Heating Characteristics and Polymerization of ε-Caprolactone Under Microwave Irradiation. *Journal of applied polymer science*, 90(10), 2657–2664

[24] Nguyen, N. T., Greenhalgh, E., Kamaruddin, M. J., El Harfi, J., Carmicheal, K., Dimitrakis, G., Kingman, S. W., Robinson, J. P., Irvine, D. J. (2014). Understanding the acceleration in the ring-opening of lactones delivered by microwave heating. *Tetrahedron*, 70(4), 996–1003

[25] Liao, L. Q., Liu, L. J., Zhang, C., He, F., Zhuo, R. X., Wan, K. (2002). Microwave-assisted ring-opening polymerization of ε-caprolactone. *Journal of Polymer Science, Part A: Polymer Chemistry*, 40(11), 1749–1755

[26] Yamada, S., Takasu, A., Kawamura, K. (2013). The effect of microwave irradiation on the kinetics and activation thermodynamics of ring-opening polymerization of ε-caprolactone. *Journal of Polymer Science, Part A: Polymer Chemistry*, 51(17), 3732–3739

[27] Thomas, C., Peruch, F., Bibal, B. (2012). Ring-opening polymerization of lactones using supramolecular organocatalysts under simple conditions. *RSC Advances*, 2(33), 12851–12856

[28] Utroša, P., Onder, O. C., Žagar, E., Kovačič, S., Pahovnik, D. (2019). Shape Memory Behavior of Emulsion-Templated Poly(ε-Caprolactone) Synthesized by Organocatalyzed Ring-Opening Polymerization. *Macromolecules*, 52(23), 9291–9298

[29] Ohn, N., Shin, J., Kim, S. S., Kim, J. G. (2017). Mechanochemical Ring-Opening Polymerization of Lactide: Liquid-Assisted Grinding for the Green Synthesis of Poly(lactic acid) with High Molecular Weight. *ChemSusChem*, 10(18), 3529–3533

[30] Kremer, A. B., Mehrkhodavandi, P. (2019). Dinuclear catalysts for the ring opening polymerization of lactide. *Coordination Chemistry Reviews*, 380, 35–57

[31] Hu, J., Kan, C., Wang, H., Ma, H. (2018). Highly Active Chiral Oxazolinyl Aminophenolate Magnesium Initiators for Isoselective Ring-Opening Polymerization of rac-Lactide: Dinuclearity Induced Enantiomorphic Site Control. *Macromolecules*, 51(14), 5304–5312

[32] Lecomte, P., Jérôme, C. (2011). Recent Developments in Ring-Opening Polymerization of Lactones. In: Rieger, B., Künkel, A., Coates, G., Reichardt, R., Dinjus, E., Zevaco, T. *Synthetic Biodegradable Polymers. Advances in Polymer Science*, vol. 245, Eds. Berlin, Heidelberg: Springer

[33] Dechy-Cabaret, O., Martin-Vaca, B., Bourissou, D. (2004). Controlled ring-opening polymerization of lactide and glycolide. *Chemical Reviews*, 104(12), 6147–6176

[34] Ajellal, N., Carpentier, J.-F., Guillaume, C., Guillaume, S. M., Helou, M., Poirier, V., Sarazin, Y., Trifonov, A. (2010). Metal-catalyzed immortal ring-opening polymerization of lactones, lactides and cyclic carbonates. *Dalton Transactions*, 39(36), 8363–8376

[35] Mazarro, R., Cabezas, L. I., de Lucas, A., Gracia, I., Rodriguez, J. F. (2009). Study of different catalysts and initiators in bulk copolymerization of d,l-lactide and glycolide. *Journal of Macromolecular Science, Part A: Pure and Applied Chemistry*, 46(11), 1049–1059

[36] Mazarro, R., de Lucas, A., Gracia, I., Rodríguez, J. F. (2008). Kinetic study of D,L-lactide and glycolide homopolymerizations by differential scanning calorimetry." *Macromolecular Chemistry and Physics*, 209(8), 818–824

[37] Dove, A. P. (2012). Organic Catalysis for Ring-Opening Polymerization. *ACS Macro Letters*, 1(12), 1409–1412

[38] Wang, X., Liu, Y., Li, Z., Wang, H., Gebru, H., Chen, S., Zhu, H., Wei, F., Guo, K. (2017). Organocatalyzed Anionic Ring-Opening Polymerizations of *N*-Sulfonyl Aziridines with Organic Superbases. *ACS Macro Letters*, 6(12), 1331-1336

[39] Labet, M., Thielemans, W. (2009). Synthesis of polycaprolactone: a review." *Chemical Society Reviews*, 38(12), 3484–3504

[40] Zhang, L., Nederberg, F., Pratt, R. C., Waymouth, R. M., Hedrick, J. L., Wade, C. G. (2007). Phosphazene Bases: A New Category of Organocatalysts for the Living Ring-Opening Polymerization of Cyclic Esters. *Macromolecules*, 40(12), 4154-4158

[41] Xu, J., Song, J., Pispas, S., Zhang, G. (2014). Controlled/living ring-opening polymerization of ε-caprolactone with salicylic acid as the organocatalyst. *Journal of Polymer Science Part A: Polymer Chemistry*, 52(8), 1185-1192

[42] Gazeau-Bureau, S., Delcroix, D., Martín-Vaca, B., Bourissou, D., Navarro, C., Magnet, S. (2008). Organo-Catalyzed ROP of ε-Caprolactone: Methanesulfonic Acid Competes with Trifluoromethanesulfonic Acid. *Macromolecules*, 41(11), 3782-3784

[43] Hege, C. S., Schiller, S. M. (2014). Non-toxic catalysts for ring-opening polymerizations of biodegradable polymers at room temperature for biohybrid materials. *Green Chemistry*, 16(3), 1410-1416

[44] Rodríguez-Tobías, H., Morales, G., Enríquez-Medrano, F. J., Grande, D. (2017). Performance of Zinc Oxide Nanoparticles as Polymerization Initiating Systems in the Microwave-Assisted Synthesis of Poly(d,l-Lactide)/ZnO Nanocomposites. *Macromolecular Symposia*, 374(1), 1600102

[45] Wu, F., Chen, S., Tang, T., Fang, H., Tian, H., Li, D., Peng, X. (2020). Thermal conductivity of polycaprolactone/three-dimensional hexagonal boron nitride composites and multi-orientation model investigation. *Composites Science and Technology*, 197, 108245

[46] Martínez-Gallegos, S., Herrero, M., Rives, V. (2008). *In situ* microwave-assisted polymerization of polyethylene terephtalate in layered double hydroxides. *Journal of Applied Polymer Science*, 109(3), 1388–1394

[47] Herrero, M.. Martínez-Gallegos, S., Labajos, F. M., Rives, V. (2011). Layered double hydroxide/polyethylene terephthalate nanocomposites. Influence of the intercalated LDH anion and the type of polymerization heating method. *Journal of Solid State Chemistry*, 184(11), 2862–2869

[48] Vasile, E., Radu, I.-C., Galateanu, B., Rapa, M., Hudita, A., Jianu, D., Stanescu, P.-O., Cioflan, H., Zaharia, C. (2020). Novel Nanocomposites Based on Bacterial Polyester/LDH-SDS Clay for Stem Cells Delivery in Modern Wound Healing Management. *Materials*, 13(20), 4488

[49] Chiang, M.-F., Wu, T.-M. (2010). Synthesis and characterization of biodegradable poly(l-lactide)/layered double hydroxide nanocomposites. *Composites Science and Technology*, 70(1), 110-115

[50] Peng, H., Han, Y., Liu, T., Tjiu, W. C., He, C. (2010). Morphology and thermal degradation behavior of highly exfoliated CoAl-layered double hydroxide/polycaprolactone nanocomposites prepared by simple solution intercalation. *Thermochimica Acta*, 502(1–2), 1-7

[51] Tsai, T.-Y., Naveen, B., Shiu, W.-C., Lu, S.-W. (2014). An advanced preparation and characterization of the PET/MgAl-LDH nanocomposites. *RSC Advances*, 4(49), 25683-25691

[52] Totaro, G., Sisti, L., Celli, A., Aloisio, I., Di Gioia, D., Marek, A. A., Verney, V., Leroux, F. (2018). Dual chain extension effect and antibacterial properties of biomolecules interleaved within LDH dispersed into PBS by: In situ polymerization. *Dalton Transactions*, 47(9), 3155–3165

[53] Katiyar, V., Gerds, N., Koch, C. B., Risbo, J., Hansen, H. C. B., Plackett, D. (2010). Poly l-lactide-layered double hydroxide nanocomposites via *in situ* polymerization of l-lactide. *Polymer Degradation and Stability*, 95(12), 2563-2573

[54] Kredatusová, J., Beneš, H., Livi, S., Pop-Georgievski, O., Ecorchard, P., Abbrent, S., Pavlova, E., Bogdał, D. (2016). Influence of ionic liquid-modified LDH on microwave-assisted polymerization of ε-caprolactone. *Polymer*, 100, 86–94

[55] Ameena Shirin, V. K., Sankar, R., Johnson, A. P., Gangadharappa, H. V., Pramod, K. (2021). Advanced drug delivery applications of layered double hydroxide. *Journal of Controlled Release*, 330, 398–426

[56] Jijoe, P. S., Yashas, S. R., Shivaraju, H. P. (2021). Fundamentals, synthesis, characterization and environmental applications of layered double hydroxides: a review. *Environmental Chemistry Letters*, 19(3), 2643–2661

[57] Yu, Y., Zheng, J., Li, J., Lu, L., Yan, J., Zhang, L., Wang, L. (2021). Applications of two-dimensional materials in food packaging. *Trends in Food Science and Technology*, 110, 443–457

[58] Xu, M., Wei, M. (2018). Layered Double Hydroxide-Based Catalysts: Recent Advances in Preparation, Structure, and Applications. *Advanced Functional Materials*, 28(47), 1802943

[59] Narasimharao, K., Lee, A., Wilson, K. (2007). Catalysts in Production of Biodiesel: A Review. *Journal of Biobased Materials and Bioenergy*, 1(1), 19–30

[60] Xu, Z. P., Zhang, J., Adebajo, M. O., Zhang, H., Zhou, C. (2011). Catalytic applications of layered double hydroxides and derivatives." *Applied Clay Science*, 53(2), 139–150

[61] Du, H., Fan, J., Miao, C., Gao, M., Liu, Y., Li. D., Feng, J. (2021). Recent Advances in Constructing Interfacial Active Catalysts Based on Layered Double Hydroxides and Their Catalytic Mechanisms. *Transactions of Tianjin University*, 27(1), 24–41

[62] Seidi, F., Jouyandeh, M., Paran, S. M. R., Esmaeili, A., Karami, Z., Livi, S., Habibzadeh, S., Vahabi, H., Ganjali, M. R., Saeb, M. R. (2021). Imidazole-functionalized nitrogen-rich Mg-Al-CO_3 layered double hydroxide for developing highly crosslinkable epoxy with high thermal and mechanical properties. *Colloids and Surfaces A: Physicochemical and Engineering Aspects*, 611, 125826

[63] Cocheci, L., Lupa, L., Ţolea, N. S., Muntean, C., Negrea, P. (2020). Sequential use of ionic liquid functionalized Zn-Al layered double hydroxide as adsorbent and photocatalyst. *Separation and Purification Technology*, 250, 117104

[64] Lyu, H., Ling, Y., Fan, J., Chen, Y., Yu, Y., Xie, Z. (2019). Preparation of ionic liquid-functionalized layered double hydroxide via thiol-ene click chemistry for highly efficient removal of azo dyes during broad pH range. *Journal of Cleaner Production*, 211, 1026–1033

[65] Seftel, E. M., Ciocarlan, R. G., Michielsen, B., Meynen, V., Mullens, S., Cool, P. (2018). Insights into phosphate adsorption behavior on structurally modified ZnAl layered double hydroxides. *Applied Clay Science*, 165, 234–246

[66] Lupa, L., Cocheci, L., Pode, R., Hulka, I. (2018). Phenol adsorption using Aliquat 336 functionalized Zn-Al layered double hydroxide. *Separation and Purification Technology*, 196, 82–95

[67] Tafazoli, Z., Tehrani, M. S., Husain, S. W., Azar, P. A. (2017). Ionic liquid grafted on layered double hydroxide nanomaterial as a hydrophobic/ion-exchange adsorbent for efficient removal of azo dye. *Desalination and Water Treatment*, 99, 322–329

[68] Alhumaimess, M. S., Alsohaimi, I. H., Hassan, H. M. A., El-Sayed, M. Y., Alshammari, M. S., Aldosari, O. F., Alshamari, H. M., Kamel, M. M. (2020). Synthesis of ionic liquid intercalated layered double hydroxides of magnesium and aluminum: A greener catalyst of Knoevenagel condensation. *Journal of Saudi Chemical Society*, 24(3), 321–333

[69] Wu, Z., Xie, Z., Wang, J., Yu, T., Wang, Z., Hao, X., Abudula, A., Guan, G. (2020). Lithium-Salt-Containing Ionic Liquid-Incorporated Li-Al-Layered Double Hydroxide-Based Solid Electrolyte with High-Performance and Safety in Solid-State Lithium Batteries. *ACS Sustainable Chemistry and Engineering*, 8(33), 12378–12387

[70] Zhou, J., Sun, G., Pan, J., Pan, Y., Wang, S., Zhai, H. (2019). A nanocomposite consisting of ionic liquid-functionalized layered Mg(II)/Al(III) double hydroxides for simultaneous

electrochemical determination of cadmium(II), copper(II), mercury(II) and lead(II). *Microchimica Acta*, 186(12), 767
[71] Kubisa, P. (2009). Ionic liquids as solvents for polymerization processes — Progress and challenges. *Progress in Polymer Science*, 34(12), 1333–1347
[72] Steinrück H.-P., Wasserscheid, P. (2015). Ionic Liquids in Catalysis. *Catalysis Letters*, 145(1), 380–397
[73] Kubisa, P. (2020). Kinetics of radical polymerization in ionic liquids. *European Polymer Journal*, 133, 109778
[74] Zhao, H. (2018). Enzymatic ring-opening polymerization (ROP) of polylactones: roles of non-aqueous solvents. *Journal of Chemical Technology & Biotechnology*, 93(1), 9–19
[75] Lu, J., Yan, F., Texter, J. (2009). Advanced applications of ionic liquids in polymer science. *Progress in Polymer Science*, 34(5), 431–448
[76] Oshimura, M., Takasu, A., Nagata, K. (2009). Controlled Ring-Opening Polymerization of ε-Caprolactone Using Polymer-Supported Scandium Trifluoromethanesulfonate in Organic Solvent and Ionic Liquids. *Macromolecules*, 42(8), 3086–3091
[77] Yu, Z. J., Liu, L. J., Zhuo, R. X. (2003). Microwave-improved polymerization of ε-caprolactone initiated by carboxylic acids. *Journal of Polymer Science Part A: Polymer Chemistry*, 41(1), 13–21
[78] Liao, L., Liu, L., Zhang, C., Gong, S. (2006). Microwave-Assisted Ring-Opening Polymerization of ε-Caprolactone in the Presence of Ionic Liquid. *Macromolecular Rapid Communications*, 27(24), 2060–2064
[79] Megevand, B., Pruvost, S., Lins, L. C., Livi, S., Gérard, J.-F., Duchet-Rumeau, J. (2016). Probing nanomechanical properties with AFM to understand the structure and behavior of polymer blends compatibilized with ionic liquids. *RSC Advances*, 6(98), 96421–96430
[80] Lins, L. C., Livi, S., Duchet-Rumeau, J., Gérard, J.-F. (2015). Phosphonium ionic liquids as new compatibilizing agents of biopolymer blends composed of poly(butylene-adipate-co-terephtalate)/poly(lactic acid) (PBAT/PLA). *RSC Advances*, 5(73), 59082–59092
[81] Zhou, Y., Qiu, S., Waterhouse, G. I. N., Zhang, K., Xu, J. (2021). Enhancing the properties of PBAT/PLA composites with novel phosphorus-based ionic liquid compatibilizers. *Materials Today Communications*, 27, 102407
[82] Lopes Pereira, E. C., Farias da Silva, J. M., Jesus, R. B., Soares, B. G., Livi, S. (2017). Bronsted acidic ionic liquids: New transesterification agents for the compatibilization of polylactide/ethylene-co-vinyl acetate blends. *European Polymer Journal*, 97, 104–111
[83] Shamsuri, A. A., Jamil, S. N. A. M. (2020). Compatibilization Effect of Ionic Liquid-Based Surfactants on Physicochemical Properties of PBS/Rice Starch Blends: An Initial Study. *Materials*, 13(8), 1885
[84] Demétrio da Silva, V., Jacobi, M. M., Schrekker, H. S., Amico, S. C. (2019). Imidazolium ionic liquid compatibilizers in melt-blended styrene-butadiene rubber/aramid pulp composites. *Polymer Bulletin*, 76(7), 3451–3462
[85] Yousfi, M., Livi, S., Dumas, A., Crépin-Leblond, J., Greenhill-Hooper, M., Duchet-Rumeau, J. (2015). Ionic compatibilization of polypropylene/polyamide 6 blends using an ionic liquids/nanotalc filler combination: morphology, thermal and mechanical properties. *RSC Advances*, 5(57), 46197–46205
[86] Lopes Pereira, E. C., Soares, B. G., Silva, A. A., Farias da Silva, J. M., Barra, G. M. O., Livi, S. (2019). Conductive heterogeneous blend composites of PP/PA12 filled with ionic liquids treated-CNT. *Polymer Testing*, 74, 187–195
[87] Bischoff, E., Simon, D. A., Schrekker, H. S., Lavorgna, M., Ambrosio, L., Liberman, S. A., Mauler, R. S. (2016). Ionic liquid tailored interfaces in halloysite nanotube/heterophasic ethylene–propylene copolymer nanocomposites with enhanced mechanical properties. *European Polymer Journal*, 82, 82–92
[88] Donato, K., Matějka, L., Mauler, R. S., Donato, R. (2017). Recent Applications of Ionic Liquids in the Sol-Gel Process for Polymer–Silica Nanocomposites with Ionic Interfaces. *Colloids and Interfaces*, 1(1), 5

[89] Lins, L. C., Bugatti, V., Livi, S., Gorrasi, G. (2018). Ionic Liquid as Surfactant Agent of Hydrotalcite: Influence on the Final Properties of Polycaprolactone Matrix. *Polymers*, 10(1), 44

[90] Bugatti, V., Viscusi, G., Di Bartolomeo, A., Iemmo, L., Zampino, D. C., Vittoria, V., Gorrasi, G. (2020). Ionic Liquid as Dispersing Agent of LDH-Carbon Nanotubes into a Biodegradable Vinyl Alcohol Polymer. *Polymers*, 12(2), 495

[91] Lins, L. C., Bugatti, V., Livi, S., Gorrasi, G. (2018). Phosphonium ionic liquid as interfacial agent of layered double hydroxide: Application to a pectin matrix." *Carbohydrate Polymers*, 182, 142–148

[92] Ranu B. C., Banerjee, S. (2005). Ionic Liquid as Catalyst and Reaction Medium. The Dramatic Influence of a Task-Specific Ionic Liquid, [bmIm]OH, in Michael Addition of Active Methylene Compounds to Conjugated Ketones, Carboxylic Esters, and Nitriles. *Organic Letters*, 7(14), 3049–3052

[93] Sheldon, R. (2001). Catalytic Reaction in Ionic Liquids. *Chemical Communications*, 23, 2399–2407

[94] Ding, S., Radosz, M., Shen, Y. (2005). Ionic Liquid Catalyst for Biphasic Atom Transfer Radical Polymerization of Methyl Methacrylate. *Macromolecules*, 38(14), 5921–5928

[95] Biedroń, T., Kubisa, P. (2001). Atom-transfer radical polymerization of acrylates in an ionic liquid. *Macromolecular Rapid Communications*, 22(15), 1237–1242

[96] Lyu, Q., Yan, H., Li, L., Chen, Z., Yao, H., Nie, Y. (2017). Imidazolium Ionic Liquid Modified Graphene Oxide: As a Reinforcing Filler and Catalyst in Epoxy Resin. *Polymers*, 9(9), 447

[97] Zahmatkesh, S. (2011). Ionic liquid catalyzed synthesis and characterization of heterocyclic and optically active poly (amide-imide)s incorporating l-amino acids. *Amino Acids*, 40(2), 533–542

[98] Bartlewicz, O., Dąbek, I., Szymańska, A., Maciejewski, H. (2020). Heterogeneous Catalysis with the Participation of Ionic Liquids. *Catalysts*, 10(11), 1227

[99] Kaoukabi, A., Guillen, F., Qayouh, H., Bouyahya, A., Balieu, S., Belachemi, L., Gouhier, G., Lahcini, M. (2015). The use of ionic liquids as an organocatalyst for controlled ring-opening polymerization of ε-caprolactone. *Industrial Crops and Products*, 72, 16–23

[100] Cruz, P., Pérez, Y., del Hierro, I., Fernández-Galán, R., Fajardo, M. (2016). ε-Caprolactone polymerization using titanium complexes immobilized onto silica based materials functionalized with ionic liquids: insights into steric, electronic and support effects. *RSC Advances*, 6(24), 19723–19733

[101] Beneš, H., Kredatusová, J., Peter, J., Livi, S., Bujok, S., Pavlova, E., Hodan, J., Abbrent, S., Konefał, M., Ecorchard, P. (2019). Ionic liquids as delaminating agents of layered double hydroxide during *in-situ* synthesis of poly (butylene adipate-co-terephthalate) nanocomposites. *Nanomaterials*, 9(4), 618

[102] Bujok, S., Konefał, M., Abbrent, S., Pavlova, E., Svoboda, J., Trhliková, O., Walterová, Z., Beneš, H. (2020). Ionic liquid-functionalized LDH as catalytic-initiating nanoparticles for microwave-activated ring opening polymerization of ε-caprolactone. *Reaction Chemistry and Engineering*, 5(3), 506–518

[103] Bujok, S., Hodan, J., Beneš, H. (2020). Effects of immobilized ionic liquid on properties of biodegradable polycaprolactone/LDH nanocomposites prepared by *in situ* polymerization and melt-blending techniques. *Nanomaterials*, 10(5), 969

[104] Bujok, S., Peter, J., Halecký, M., Ecorchard, P., Machálková, A., Santos Medeiros, G., Hodan, J., Pavlova, E., Beneš, H. (2021). Sustainable microwave synthesis of biodegradable active packaging films based on polycaprolactone and layered ZnO nanoparticles. *Polymer Degradation and Stability*, 190, 109625

[105] Jin S.-E., Jin, H.-E. (2021). Antimicrobial Activity of Zinc Oxide Nano/Microparticles and Their Combinations against Pathogenic Microorganisms for Biomedical Applications: From Physicochemical Characteristics to Pharmacological Aspects. *Nanomaterials*, 11(2), 263